DASA-1892-2

Weapons Radiation Shielding Handbook

Chapter 4 / Neutron and Gamma-Ray Albedos

by Wade E. Selph

Handbook Editors

Lorraine S. Abbott, H. Clyde Claiborne, and Charles E. Clifford

DEFENSE ATOMIC SUPPORT AGENCY

Washington, D. C. 20301

DASA-1892-2

WEAPONS RADIATION SHIELDING HANDBOOK

Chapter 4. Neutron and Gamma-Ray Albedos

by
Wade E. Selph

Handbook Editors
Lorraine S. Abbott, H. Clyde Claiborne, and Charles E. Clifford

DEFENSE ATOMIC SUPPORT AGENCY
Washington, D.C. 20301

JUNE 1967

Preparing Agency
OAK RIDGE NATIONAL LABORATORY
Oak Ridge, Tennessee
Operated by UNION CARBIDE CORPORATION
for the U.S. ATOMIC ENERGY COMMISSION
DASA Order No. EO-806-65,
Task A2-11.033

Preface

At the request of the Defense Atomic Support Agency, Oak Ridge National Laboratory has undertaken the preparation of a handbook to aid engineers charged with the responsibility of designing shields to protect military equipment and personnel in the vicinity of a nuclear weapons burst. This document constitutes the second chapter of the Handbook issued thus far, the first one being Chapter 5, entitled "Methods for Calculating Effects of Ducts, Access Ways, and Holes in Shields." These two chapters, together with an introductory first chapter, will eventually be combined with a chapter defining the radiation sources insofar as is possible and practicable (Chapter 2) and a chapter outlining methods for calculating the attenuation of weapons radiation through various media (Chapter 3) to form Volume I of the Handbook. Volume II will consist of two or more additional chapters presenting engineering design methods that are based on the more sophisticated techniques described in Volume I. The intent is that the shield designer will use Volume I as a textbook and ready reference and Volume II as a guide for handling most of the problems with which he will be confronted.

In order to prepare this Handbook, it has been necessary for Oak Ridge National Laboratory to obtain the assistance of several consultants and subcontractors. For this chapter on albedos, for example, Wade E. Selph of Radiation Research Associates, Inc., performed the initial literature search and prepared the draft with which the editors worked. Other chapters will similarly represent a cooperative effort of ORNL and other organizations.

As is always the case for handbooks, the authors and editors are relying heavily on suggestions, reviews, and criticisms of others as an aid in the development of the various chapters. The list of individuals who have contributed in this manner has already grown very large, and it would be almost impossible to acknowledge each person here. We do, however, wish to express appreciation to Lt. Cols. Charles D. Daniel and William A. Alfonte, who as past DASA Shielding Project Officers handled the early administration of the contract and assisted in establishing the scope of the Handbook. The work they began is currently being ably performed by Captain R. W. Enz. We also wish to acknowledge the assistance of R. E. Maerker of Oak Ridge National Laboratory, who, by virtue of having worked on neutron albedos in recent years, has been able to serve as an on-the-spot authority to help resolve problem areas as they arose in this chapter, particularly in Sections 4.1 and 4.2.

Finally, we wish to thank Mrs Virginia M. Hamrick, who by carefully reading each draft of this chapter, including galley and page proofs, has both improved the rhetoric and helped eliminate some of the usual errors that are inevitably found in formal publications.

May 1967

Contents

4.0 Introduction

It is pointed out in Chapter 5 and elsewhere in this Handbook that an air-filled opening through a shield can increase the total amount of radiation penetrating the shield. This is not only because air affords little attenuation but also because neutrons and gamma rays can scatter successively from the walls of such openings and thus penetrate much deeper into the shield than would be possible if they traveled through shielding material alone. The problem of wall-scattered radiation is particularly acute in weapons radiation shields, which nearly always contain large ducts or passageways. Consequently, a number of studies have recently been carried out to determine the fraction of nuclear radiation incident on a material surface that is reflected back out of the material. This fraction is called the material *albedo.*

When applied to nuclear radiation, the definition of the term "albedo" is much broader than the traditional definition. For example, nuclear radiation albedos include radiation that is scattered at depths as great as or greater than a relaxation length, rather than from just the surface of the medium, since particles scattering at these depths have been shown to contribute significantly to the total radiation emerging from the surface. Also, some nuclear radiation albedos refer to mixed radiations, that is, to emergent particles of one type that result from the interaction of incident particles of another type. Such albedos might be more properly referred to as effective albedos, with the emergent radiation identified as a particular type of secondary radiation. For example, effective capture gamma-ray albedos are albedos specifying the gamma-ray dose emerging from a medium that is due to incident neutrons being captured within the medium. This type of albedo is especially important since for some duct configurations the capture gamma-ray doses can exceed the scattered neutron doses.

Theoretically, calculations of nuclear radiation albedos should be straightforward, since a large body of information is available on interaction probabilities, the angular distribution of scattered radiation, and the emergent energy versus scattering angle for a variety of incident energies and materials. But even though the single-event probabilities are well known, solution of the macroscopic multicollision albedo problem is quite complex. Consequently, the value of the single-event probabilities lies primarily in their usefulness in predicting trends. For example, if the ratio of the scattering cross section to the absorption cross section is high, as it is in the case of neutrons diffusing in concrete, the resulting albedo will tend to be high. If, however, the scattering is predominantly in the forward direction, as in the case of high-energy gamma rays, then there is a greater probability for a low albedo.

The material most frequently used in albedo investigations is concrete, since the prevalent interest is in concrete as a structural material for shelters. Other materials have been studied, such as water, iron, lead, borated polyethylene, aluminum, and various soils, but the data available for each are meager. The investigations themselves have largely consisted of calculations, primarily Monte Carlo machine calculations; however, in many cases there has been sufficient experimental confirmation to establish the validity of the calculated data. In nearly all cases the calculated data have been fitted to empirical expressions.

Because the shield designer is interested in the dose resulting from the reflected radiation, the incident and emergent particle fluxes and currents are often expressed in dose units. As a result of the differences in the energy dependence of the flux-to-dose response functions for neutrons and gamma rays, neutron dose albedos are more

strongly related to the number of particles reflected, while gamma-ray dose albedos are more strongly related to the total energy reflected.

The summarization in this chapter of the albedo data that have been obtained to date emphasizes the gaps that still exist. It will be apparent, for example, that while calculated neutron albedos for concrete are available for essentially all energy regions of interest, those for the intermediate-energy region lack experimental confirmation. Experimental confirmation of gamma-ray albedo calculations is even more limited, since all the experiments have been performed with the low gamma-ray energies that can be obtained from isotope sources. In the case of secondary gamma-ray albedos, there has been almost no experimental confirmation. On the other hand, as the list of references at the end of the chapter will reveal, the subject of nuclear radiation reflection has received a great deal of attention since 1960, and the fact that so much data has been amassed in these few years underscores the importance shield designers attach to albedos. Unfortunately, so many studies being carried out simultaneously has resulted in a diversity of nomenclature and definitions which has complicated comparisons between what should be similar data. In an attempt to alleviate this problem, all albedo data quoted in this chapter have been classified according to the definitions given in Section 4.1, which, if generally accepted, should aid in the understanding of future studies.

4.1 Definitions

4.1.1. GENERAL CONSIDERATIONS

Traditionally, albedo refers to the ratio of the radiation current reflected from a surface to the current incident on that surface. Consider, for example, a monodirectional source of radiation of energy E_0 incident on a surface at polar angle θ_0 (see Fig. 4.1). The reflected current of energy E per unit energy per unit solid angle at polar angle θ and azimuthal angle ϕ is given by

$$J(E,\theta,\phi) = J(E_0,\theta_0)\,\alpha(E_0,\theta_0,E,\theta,\phi)\,, \qquad (4.1)$$

where $J(E_0,\vartheta_0)$ is the incident current and $\alpha(E_0, \theta_0,E,\theta,\phi)$ is the albedo.

When applied to nuclear radiation, albedo is not always expressed as the ratio of the reflected current per incident current, but instead may be given as the ratio of reflected current per unit incident flux, of reflected dose per unit incident current, of reflected dose per incident dose, etc. Unlike the reflection of light which can be considered to be a surface phenomenon, neutrons and gamma rays

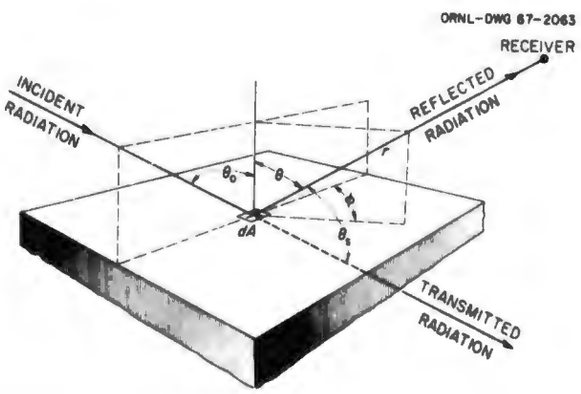

Fig. 4.1. Geometry for Calculating Neutron and Gamma-Ray Reflection from a Surface.

are much more penetrating and their albedos take into account radiation that is scattered back out of the medium from several mean free paths below the surface. The basic assumption is made that the particles emerge from the medium at the same points on the surface at which they were incident, which simplifies the use of predetermined albedos

in various calculations, such as the duct transmission problems discussed in Chapter 5.

Neutron and gamma-ray albedos are available in several forms. The form used in Eq. 4.1 is doubly differential; that is, it is differential with respect to both the reflected energy E and the reflected direction (as determined by θ and ϕ). A singly differential albedo results when a doubly differential albedo is integrated over either energy or direction. Dose albedos obtained experimentally as a function of exit directions are also examples of singly differential albedos since dose is an integral quantity with respect to energy. The term "total albedo" always implies that integration has been performed over both energy and direction. In this Handbook, differential albedos are denoted by the symbol α, as in Eq. 4.1, and total albedos by the symbol A.

Three different types of differential and total albedos have been used by various investigators in reporting their results on material reflectivity. The first type, denoted here by the subscript 1, is an albedo which represents an incident flux of particles and an emergent current. The second and third types, denoted by subscripts 2 and 3, are albedos for which the incident and emergent particles are considered to be the same – current for the type 2 albedo and flux for the type 3 albedo. Fluxes and currents are related functionally by the cosine of the entrance or exit angles. For example, if $\Phi(E,\theta,\phi)$ is the reflected differential flux per unit energy per steradian, then the reflected current per unit energy per steradian, $J(E,\theta,\phi)$, is equal to $\Phi(E,\theta,\phi) \cos\theta$.

If the albedo being considered represents some weighting of the particle flux such as dose or energy flux, then the subscripted letter D or E will precede the numerical subscript. In the albedo definitions given below, the term "dose" or "dose rate" is used in the generic sense. The albedo definitions are not affected by the various types or names of doses that are used. The choice of the dose definition and the flux-to-dose conversion ratio govern whether the doses are exposure dose, absorbed dose, kerma, dose equivalent, single-collision dose, or multicollision dose (see Chapter 1). Standard functional notation is used in conjunction with the albedo symbols to designate the independent variables for the particular albedo being considered.

4.1.2. DIFFERENTIAL DOSE ALBEDOS

The definitions of the three types of differential albedos for which the particle flux has been weighted by a dose response function are as follows:

$\alpha_{D1}(E_0,\theta_0,\theta,\phi)$, **Differential Current Out (in Dose Units) per Incident Flux (in Dose Units).** – If the dose due to particles of energy E_0 incident at angle θ_0 is D_0, then the particle current (in dose units) per steradian reflected in the direction θ,ϕ is given by $D_0\alpha_{D1}$. The reflected particle current in dose units (or dose current) has no physical meaning but is merely a mathematical convenience. It is expressed mathematically by

$$D(\theta,\phi) = \int K(E)\, J(E,\theta,\phi)\, dE\,, \qquad (4.2)$$

where $J(E,\theta,\phi) = \Phi(E,\theta,\phi) \cos\theta$ and $K(E)$ is the *flux*-to-dose conversion factor for particles of energy E. The current measuring plane in these definitions is the material interface plane.

$\alpha_{D2}(E_0,\theta_0,\theta,\phi)$, **Differential Current Out (in Dose Units) per Incident Current (in Dose Units).** – If the dose due to particles of energy E_0 incident at angle θ_0 is D_0 (flux in dose units), then the particle current (in dose units) per steradian reflected in the direction θ,ϕ is given by $D_0 \cos\theta_0\, \alpha_{D2}$, where $D_0 \cos\theta_0$ is the incident particle current in dose units. This type differs from the traditional current albedo only in that the current is weighted by a dose response function.

$\alpha_{D3}(E_0,\theta_0,\theta,\phi)$, **Differential Flux Out (in Dose Units) per Incident Flux (in Dose Units).** – If the dose due to particles of energy E_0 incident at angle θ_0 is D_0, then the dose per steradian due to particles reflected in the direction θ,ϕ is $D_0\alpha_{D3}$. If the incident particle current per unit surface area is $J(E_0)$, then $D_0 = K(E_0)\, J(E_0) \sec\theta_0$. If the reflected particle current per unit surface area is $J(E,\theta,\phi)$, then the reflected differential dose is

$$D(\theta,\phi) = \int K(E)\, J(E,\theta,\phi) \sec\theta\, dE\,, \qquad (4.3)$$

where $D(\theta,\phi)$ is the dose per steradian due to particles reflected in the direction θ,ϕ.

The three types of albedos defined above are related by

$$\alpha_{D1} = \alpha_{D2} \cos\theta_0 = \alpha_{D3} \cos\theta\,. \qquad (4.4)$$

4.1.3. TOTAL DOSE ALBEDOS

Total dose albedos are obtained by integrating differential dose albedos over the solid angle represented by the exit hemisphere. Thus the three types of total dose albedos corresponding to the differential albedos described above are defined by

$$A_{D1}(E_0,\theta_0) = \int \alpha_{D1}(E_0,\theta_0,\theta,\phi)\, d\Omega\,, \qquad (4.5)$$

$$A_{D2}(E_0,\theta_0) = \int \alpha_{D2}(E_0,\theta_0,\theta,\phi)\, d\Omega$$

$$= \sec\theta_0 \int \alpha_{D1}(E_0,\theta_0,\theta,\phi)\, d\Omega\,, \qquad (4.6)$$

$$A_{D3}(E_0,\theta_0) = \int \alpha_{D3}(E_0,\theta_0,\theta,\phi)\, d\Omega$$

$$= \int \alpha_{D1}(E_0,\theta_0,\theta,\phi) \sec\theta\, d\Omega$$

$$= \cos\theta_0 \int \alpha_{D2}(E_0,\theta_0,\theta,\phi) \sec\theta\, d\Omega\,, \qquad (4.7)$$

where $d\Omega = \sin\theta\, d\theta\, d\phi$ and the limits of integration are from $\theta = 0$ to $\pi/2$ and from $\phi = 0$ to 2π.

Differential data must be available when data for A_{D3} are being compared with the other two types of total albedos, whereas A_{D1} and A_{D2} are directly related; i.e., $A_{D1} = \cos\theta_0 A_{D2}$.

4.1.4. OTHER ALBEDOS

Particle flux or current and energy flux or current albedos, which refer either to particle or energy flow, have also been used. In keeping with the previous nomenclature, these are

A_1 or α_1 = particle current out per unit particle flux in,

A_2 or α_2 = particle current out per unit particle current in,

A_3 or α_3 = particle flux out per unit particle flux in.

For the case in which energy flow is considered, these particle flow quantities are weighted by the energy and

A_{E1} or α_{E1} = energy current out per unit energy flux in, etc.

All the parameters involved in these albedo definitions are the same as in the dose albedo definitions except that neither the incident nor the reflected flux (or current) is converted to dose units.

4.1.5. APPLICATION

Basic data on radiation reflection find many applications in the analysis of protective structures, the reflected radiation in some cases being the primary consideration. An example of how such data can be used is as follows.

Consider a detector positioned at an entranceway with a surrounding concrete pad exposed to an elevated monoenergetic point source of radiation as shown in Fig. 4.2. The total response at P

ORNL-DWG 67-4074

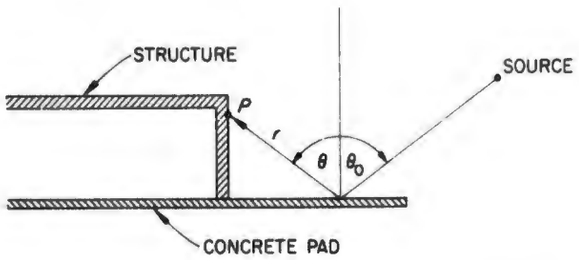

Fig. 4.2. Geometry for Calculating Radiation Scattered into a Structure.

will be due to the radiation that travels directly from the source plus the radiation which scatters to P from the air, the ground, or the concrete. (The scattered component will include radiation that has been multiply scattered from some combination of these three media; however, in most cases of interest, multiple-medium scattering may be neglected with little loss in accuracy.) The ground- and concrete-scattered components may be evaluated by performing a numerical integration of the product of the incident intensity and the material albedo over the exposed surface area. For example, if a type 1 albedo for concrete is used, the dose at the detector due to scattering from the concrete pad will be given by

$$D = \int \frac{D_0}{r^2}\, \alpha_{D1}(E_0,\theta_0,\theta,\phi)\, dS\,, \qquad (4.8)$$

where D_0 is the incident dose at an incremental area dS, r is the distance between P and the point of reflection from the pad, and the integration is over the concrete area viewed by the detector.

If a type 2 or type 3 albedo is used, Eq. 4.8 becomes

$$D = \int \frac{D_0 \cos\theta_0}{r^2} \alpha_{D2}(E_0,\theta_0,\theta,\phi)\, dS \qquad (4.9)$$

and

$$D = \int \frac{D_0 \cos\theta}{r^2} \alpha_{D3}(E_0,\theta_0,\theta,\phi)\, dS\,, \qquad (4.10)$$

respectively.

The dose at a point on the concrete-air interface may be obtained by using

$$D = D_0\,[1 + A_{D3}(E_0,\theta_0)] = D_0 \left[1 + \int_0^{2\pi}\int_0^{\pi/2} \alpha_{D3}(E_0,\theta_0,\theta,\phi) \sin\theta\, d\theta\, d\phi\right]. \qquad (4.11)$$

If the radiation spectrum at the detector is desired, a more complex form of the albedo (such as a flux or current albedo or a dose albedo that is differential in exit energy) is used, and the integration becomes more complex. For example, it is necessary to integrate over the incident energy spectrum and to accumulate the reflected contributions into energy groups which form the reflected spectrum.

4.2 Neutron Albedos

The fundamental mechanisms which result in neutrons being scattered backwards in a material are elastic and inelastic scattering, the two processes being distinguished by the condition of the target nucleus following its collision with the neutron. In an elastic scattering the total kinetic energy of the incident particle and the target nucleus is unchanged, and the nucleus is left in the same internal state as before the collision. In an inelastic scattering the total kinetic energy is decreased, and the nucleus is left in an excited state. In either case an intermediate step may be the formation of a very short-lived compound nucleus, from which the original neutron, or its replacement, is immediately ejected.

As a result of many successive scatterings, neutrons can follow tortuous paths which are difficult to calculate. Nevertheless calculations of neutron albedos have been successfully performed with experimental confirmation in a number of cases. The investigations have fallen into three major categories, distinguished by the energies of the reflected neutrons: fast neutrons, intermediate-energy neutrons, and thermal neutrons. The studies of thermal-neutron albedos have been further categorized as relating to albedos that result from incident thermal neutrons and those that result from neutrons incident at energies higher than thermal energy. Since neutrons that are incident at thermal energy scatter in a much more orderly process than do higher energy neutrons, this category has yielded to the direct analytical approach much more readily than the other categories. In general, expressions for other types of albedos have been obtained by fits to results from machine calculations, the majority being Monte Carlo type of calculations.

From the following discussion it will be apparent that almost all the neutron albedo investigations have been for some form of concrete, although a few have also included other materials.

4.2.1. FAST-NEUTRON ALBEDOS

The major contributions to the data on fast-neutron albedos have resulted from studies made by Maerker and Muckenthaler[1] and by Allen, Futterer, and Wright.[2] Both groups performed detailed Monte Carlo calculations to determine the reflec-

tion from materials that is due to fast neutrons of various energies incident on the materials at various angles. The results of Maerker and Muckenthaler are more detailed than those of Allen *et al.* in that the reflection data are differential with respect both to the reflected direction (see Fig. 4.1) and to the reflected energy. The Allen *et al.* data are differential with respect to the direction only.

The Maerker and Muckenthaler calculations were performed as part of a calculational and experimental program that covered a wide range of neutron energies (see Sections 4.2.2 and 4.2.3) and included an investigation of secondary gamma-ray albedos (see Section 4.4). In the experimental phase, which was performed at the ORNL Tower Shielding Facility, a 9-in.-thick concrete slab was used which was reinforced with steel bars at a depth of $1\frac{1}{2}$ in. from either side. For the fast-neutron calculations (but not for the intermediate- and thermal-neutron calculations discussed later) the steel was not considered and the concrete composition was assumed to be a typical concrete of the composition shown in Table 4.1.*

The calculations were performed for six incident energy bands covering the energy range between 0.2 and 8 MeV. In a particular problem the neutrons incident on the concrete were sampled uniformly from each incident-energy band, and a statistical estimation technique was used to obtain estimates of the current emerging from the surface at various angles from a normal to the surface. The emergent angles were determined by the intersection points of a grid formed by nine space-fixed polar angles and six azimuthal angles. The results, obtained for distinct values of θ_0, θ, and ϕ, were grouped into energy bands ΔE_0 and ΔE. There were ten reflected energy bands, which, like the incident energy bands, covered the range between 0.2 and 8 MeV. (Note: Albedos that include neutrons reflected at energies less than 0.2 MeV were determined separately and are discussed in Sections 4.2.2 and 4.2.3.)

The differential albedo $\alpha_{D2}(E_0,\theta_0,E,\theta,\phi)$ calculated by Maerker and Muckenthaler is in units of reflected current (in single-collision dose units) per MeV per steradian per incident current (in single-collision dose units) of a "gun-barrel" beam source. This albedo differs from the α_{D2} discussed in Section 4.1 only in that, as was pointed out previously, it is differential with respect to the reflected energy as well as the reflected direction (that is, it is a doubly differential albedo). The statistical uncertainty associated with the Maerker-Muckenthaler data is about 10% for the doubly differential albedos and about 3% for singly differential albedos.

Typical results from these calculations are shown in Figs. 4.3 through 4.6. Figure 4.3 shows the variation of the total albedo (integrated over both the reflected energy and the reflected angle) as a function of the incident angle and incident energy band. Figures 4.4 and 4.5 show the de-

*An analysis of the concrete that was used in the experiment is shown in Table 4.5 in Section 4.2.2.

Table 4.1. Concrete Compositions Used in Monte Carlo Calculations

Element	Composition (in units of 10^{21} atoms/cm^3)	
	Maerker and Muckenthaler	Allen *et al.*
H	9.43	13.75
O	47.6	45.87
Si	11.85	20.15
Ca	7.8	
Density (g/cm^3)	2.35	2.26

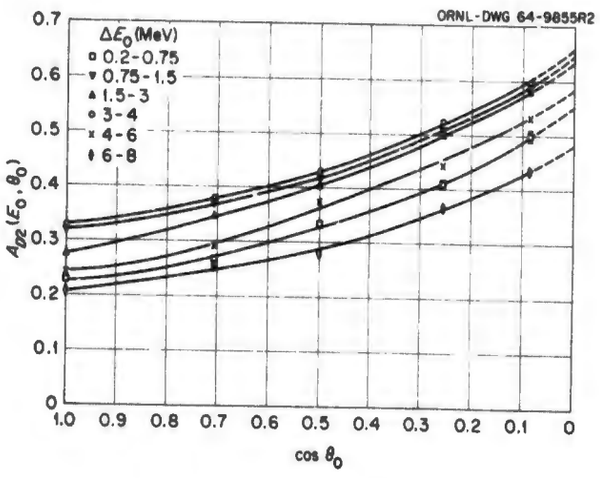

Fig. 4.3. Total Single-Collision Dose Albedo as a Function of cos θ_0 and ΔE_0 for Fast Neutrons (>0.2 MeV) Reflected from Concrete. (From Maerker and Muckenthaler, ref. 1.)

pendence of the differential dose albedo on the reflection angles θ and ϕ, Fig. 4.5 clearly illustrating that the assumption of no dependence on the reflected azimuthal angle ϕ can lead to considerable error in the differential albedo for some conditions. The dependence on the azimuthal angle is strongest for high-energy neutrons at grazing angles of incidence and emergence, becoming very weak for low-energy neutrons or for values of ϕ greater than 45 deg. This trend is consistent with what would be expected since the first scatterings of high-energy neutrons are in the forward direction and since neutrons that have scattered more than once tend to have "forgotten" their initial direction and thus emerge from the material in a rather random manner. Figure 4.6 shows how the ratio of the total dose albedo for singly scattered neutrons to the total dose albedo for singly plus multiply scattered neutrons increases with increasing values of the polar angle of incidence.

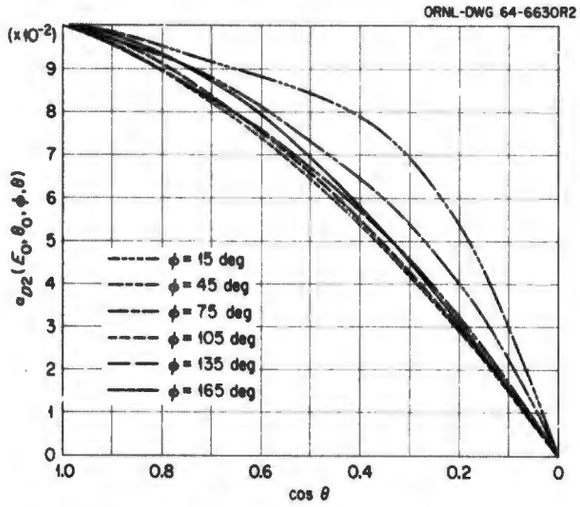

Fig. 4.4. Differential Single-Collision Dose Albedo per Steradian as a Function of cos θ and ϕ for 1.5- to 3-MeV Neutrons Incident on Concrete at θ_0 = 60 deg. (From Maerker and Muckenthaler, ref. 1.)

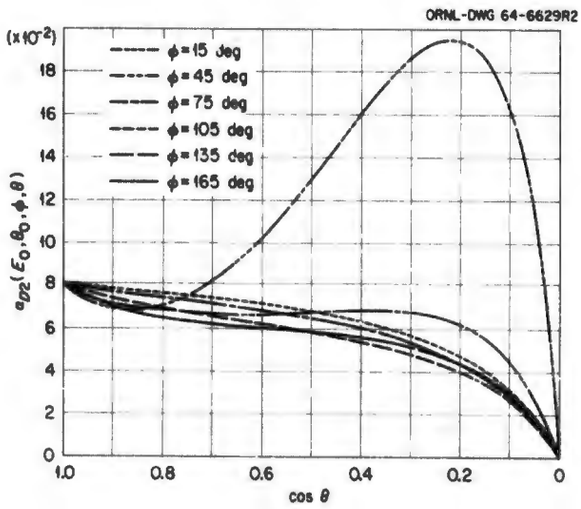

Fig. 4.5. Differential Single-Collision Dose Albedo per Steradian as a Function of cos θ and ϕ for 6- to 8-MeV Neutrons Incident on Concrete at θ_0 = 85 deg. (From Maerker and Muckenthaler, ref. 1.)

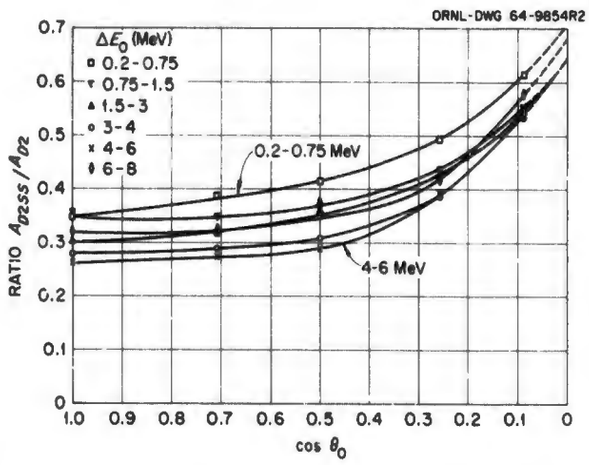

Fig. 4.6. Ratio of Total Single-Collision Dose Albedo for Fast Neutrons (>0.2 MeV) Singly Scattered from Concrete to Total Albedo for Singly Plus Multiply Scattered Neutrons as a Function of cos θ_0 and ΔE_0. (From Maerker and Muckenthaler, ref. 1.)

Maerker and Muckenthaler derived an expression to fit their angular differential dose albedo data which reproduces their Monte Carlo results within 10%. The expression involves two terms: the first accounts only for singly scattered neutrons and the second includes all multiply scattered neutrons, it being assumed that the configuration is effectively a semi-infinite body of concrete. The expression is as follows:

$$\alpha_{D2}(E_0, \theta_0, \theta, \phi) = \frac{\cos\theta}{\cos\theta + K_1(\Delta E_0)\cos\theta_0} \times$$

$$\times \sum_{m=0}^{M} G_m(\Delta E_0) P_m(\cos\theta_s) + \frac{\cos\theta}{\cos\theta + K_2(\Delta E_0,\theta_0,\theta)}$$

$$\times \sum_{k=0}^{K} B_k(\Delta E_0) P_k(\cos\theta_s) , \quad (4.12)$$

where $\cos\theta_s = \sin\theta_0 \sin\theta \cos\phi - \cos\theta_0 \cos\theta$; P_m and P_k are Legendre polynomials of orders m and k;

$$K_2(\Delta E_0,\theta_0,\theta) = \sum_{i=0}^{I} (\cos\theta)^i$$

$$\times \sum_{j=0}^{J} a_{ij}(\Delta E_0) \cos^j\theta_0 ; \quad (4.13)$$

and the constants G_m, B_k, K_1, and a_{ij} are given in Table 4.2.

Maerker and Muckenthaler also performed calculations in which their differential albedos were used to predict reflected fast-neutron doses due to a collimated beam of reactor neutrons incident at various angles on a 6-ft-square, 9-in.-thick concrete slab, and they compared the results with the reflected doses measured in an experiment performed at the ORNL Tower Shielding Facility (TSF). The values of the incident angles θ_0 covered in the calculations and the experiment were 0, 45, 60, and 75 deg. The calculations were weighted by an incident spectrum previously measured at the TSF, and the incident dose rate used was the dose rate determined by integrating the measured dose rates over the effective cross-sectional area of the incident beam.

The reflected dose rates were predicted with the equation

$$D_R(\theta_0,\theta,\phi) = \frac{D_0}{r^2} \sum_{\Delta E_0} \beta(\Delta E_0) \sum_{\Delta E} \cos\theta_0$$

$$\times \alpha_{D2}(\Delta E_0,\theta_0,\Delta E,\theta,\phi)\, e^{-\Sigma_{T,air}(\Delta E)r} , \quad (4.14)$$

where β is the fraction of D_0 lying within ΔE_0, r is the distance from the surface to the detector, and $\Sigma_{T,air}(\Delta E)$ is the average macroscopic cross section in the energy group ΔE based on the assumption of a flat flux distribution within the energy interval ΔE. The root mean square deviation between the predicted and measured values is 3.1%, and the largest single deviation is 9%. This close agreement indicates that, in spite of the differences in the compositions of the concrete assumed for the calculations and that used in the experiment, the albedo is relatively insensitive to the changes in the concrete composition within these limits.

The Monte Carlo calculations performed by Allen *et al.*[3] determined the fraction of neutrons from monoenergetic sources that was transmitted through and reflected from infinite slabs of various materials, including concrete. The source energies were 0.10, 0.25, 0.50, 1.0, 2.0, 3.5, 5.0, and 14 MeV, and the angles of incidence were 0, 30, 45, and 70 deg from the normal to the slab. The low-energy cutoff was 10 eV. Transmitted and reflected neutrons were accumulated in energy and angle intervals, the reflected data yielding the multicollision dose albedos $\alpha_{D3}(E_0,\theta_0,\theta)$ and $A_{D3}(E_0,\theta_0)$. Energy spectra of the reflected flux were also determined for each incident energy-angle combination.

In addition to concrete, the materials covered in the calculations were water, iron, 8% borated polyethylene, and three Nevada Test Site (NTS) soils differing only in moisture content. The densities and elemental content of the materials are given in Tables 4.1 and 4.3. In all cases the slabs were assumed to be sufficiently thick to yield albedo data approximating those for a semi-infinite geometry.

Typical results from the calculations of Allen *et al.* are presented in Figs. 4.7 through 4.11. Figures 4.7 through 4.9 are plots of the total dose albedos for the various materials as a function of the hydrogen content for incident source energies of 0.1, 2.0, and 14.0 MeV, respectively. Figure 4.10 shows the energy spectra of the neutrons reflected from a concrete slab due to a 3.0-MeV source incident at the various angles, and Fig. 4.11 gives the angular distributions of reflected neutrons due to a 1.0-MeV source.

French and Wells[4] analyzed the differential data of Allen *et al.* and obtained a fit that is a function of the incident and reflected polar angles only. The dependence of the reflected azimuthal angle ϕ was found to be weak and for the most part irregular; thus the dose reflection data were averaged

Table 4.2. Constants for the Expression[a] Fitting the Maerker-Muckenthaler Differential Dose Albedo Data for Fast Neutrons Incident on Concrete[b]

Constant	Value of Constant for ΔE_0 of					
	0.2 – 0.75 MeV	0.75 – 1.5 MeV	1.5 – 3 MeV	3 – 4 MeV	4 – 6 MeV	6 – 8 MeV
G_0	6.585-2[c]	7.045-2	7.211-2	7.024-2	6.856-2	5.899-2
G_1	5.048-2	4.393-2	5.845-2	7.452-2	8.294-2	6.039-2
G_2	3.710-2	7.088-2	5.968-2	1.000-1	9.517-2	7.524-2
G_3	1.544-2	1.898-2	2.729-2	5.591-2	7.761-2	8.140-2
G_4	7.837-3	2.408-3	1.190-2	2.646-2	4.292-2	6.622-2
G_5	0	−3.589-3	1.000-3	−6.908-4	1.824-2	3.056-2
G_6	0	0	4.637-3	−8.087-4	5.599-3	1.595-2
G_7	0	0	6.490-3	−1.459-3	5.288-3	1.277-2
G_8	0	0	0	−1.809-3	1.046-2	9.380-3
B_0	6.27-2	9.00-2	8.80-2	9.05-2	8.744-2	6.374-2
B_1	1.50-2	8.5-3	1.30-2	2.15-2	2.817-2	1.382-2
B_2	5.3-3	9.7-3	6.0-3	2.30-2	2.344-2	1.178-2
B_3	0	0	0	0	1.779-2	1.084-2
B_4	0	0	0	0	8.517-3	6.801-3
K_1	1.0	1.0	1.1	0.9	1.1	1.06
a_{00}	0.36	0.51	0.56	0.60	0.43	0.35
a_{01}	1.29	0.32	−0.18	0.15	2.02	0.95
a_{02}	0	1.00	1.32	0.48	−0.38	0
a_{10}	0.06	−0.04	−0.14	−0.61	0.05	0.10
a_{11}	−3.06	−2.46	−2.76	−1.08	−9.13	−2.28
a_{12}	0	0	0	0	5.93	1.11
a_{20}	−0.20	0.05	0.05	0.32	0.04	0
a_{21}	1.68	0.95	1.14	0.30	5.97	0
a_{22}	0	0	0	0	−4.39	0

[a]Equation 4.12.

[b]Table taken from: R. E. Maerker and F. J. Muckenthaler, *Nucl. Sci. Eng.* 22, 455–462 (1965).

[c]6.585×10^{-2}, etc.

Table 4.3. Compositions of Soil, Iron, and Polyethylene Used in Monte Carlo Calculations by Allen *et al.**

Element	Composition (in units of 10^{21} atoms/cm^3)				
	Nevada Test Site Soil			Iron	8% Borated Polyethylene
	Dry	50% Saturated	100% Saturated		
^{10}B					0.658
^{11}B					2.67
H	8.553	9.80	16.87		76.8
C					39.2
O	22.68	23.30	27.00		
Al	2.014	1.830	1.976		
Si	9.533	8.680	8.963		
Fe				84.9	
Density (g/cm^3)	1.15	1.12	1.25	7.88	0.97

*Table taken from: F. J. Allen, A. Futterer, and W. Wright, *Dependence of Neutron Albedos upon Hydrogen Content of a Shield*, Ballistics Research Laboratories Report BRL-1224 (October 1963).

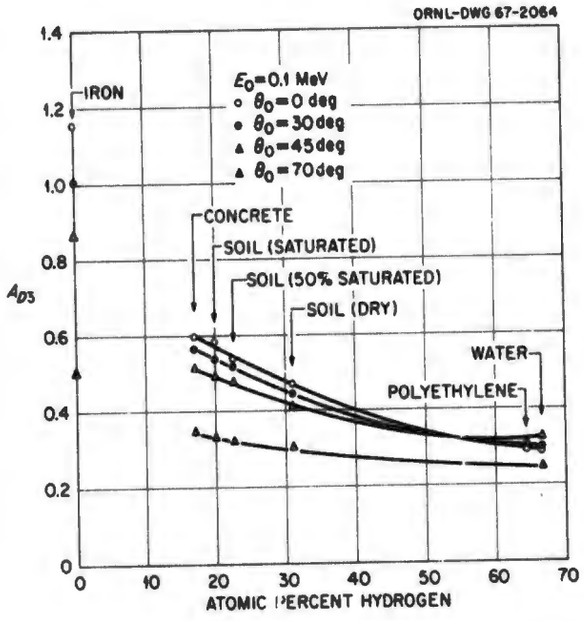

Fig. 4.7. Total Multicollision Dose Albedo for 0.1-MeV Neutrons Incident on Various Materials. (From Allen *et al.*, ref. 3.)

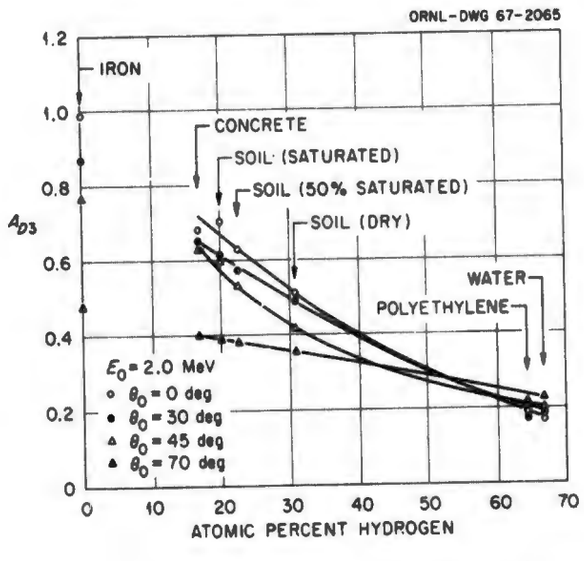

Fig. 4.8. Total Multicollision Dose Albedo for 2.0-MeV Neutrons Incident on Various Materials. (From Allen *et al.*, ref. 3.)

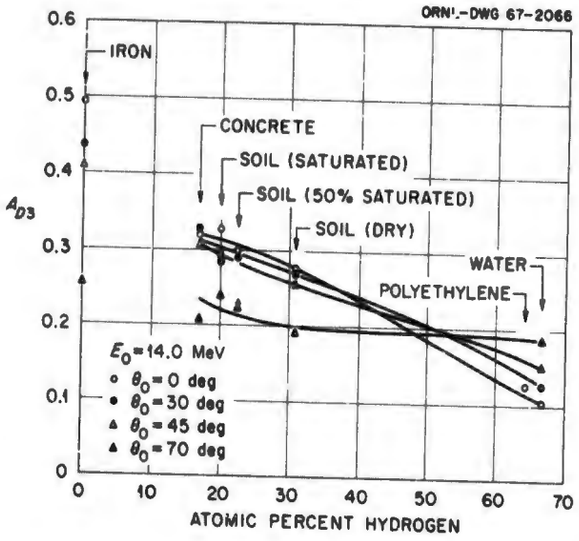

Fig. 4.9. Total Multicollision Dose Albedo for 14.0-MeV Neutrons Incident on Various Materials. (From Allen *et al.*, ref. 3.)

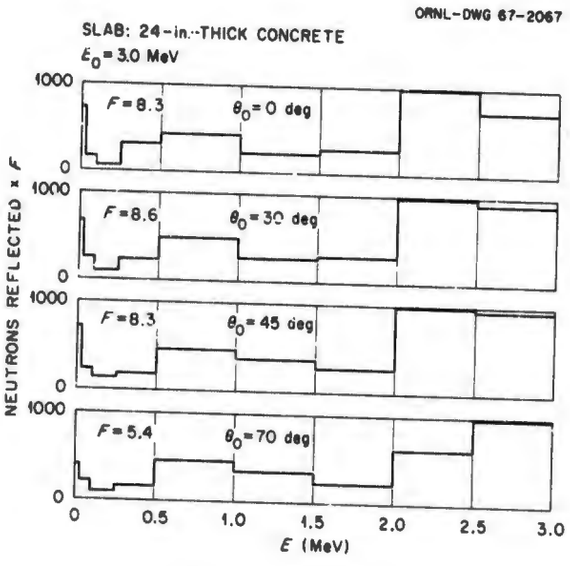

Fig. 4.10. Energy Spectrum of Fast Neutrons Reflected from Concrete (F = Arbitrary Number). (From Allen *et al.*, ref. 2.)

over ϕ. The dependence on the reflected polar angle was found to fit a cos θ function, and the dependence on the incident angle was approximated by $\cos^{2/3}\theta_0$, yielding an expression of the form*

$$\alpha_{D1} = k(E_0)\cos^{2/3}\theta_0 \cos\theta\,, \qquad (4.15)$$

where $k(E_0)$ is a normalizing constant which includes the effect of incident energy and reflecting material. Values of $k(E_0)$ are shown in Table 4.4 for concrete, the three NTS soils, and iron for eight monoenergetic sources and a fission source. Equation 4.15 is assumed to be valid for all materials of low to moderate hydrogen content ($\Sigma_H/\Sigma_T <$ 0.5). (The water data of Allen *et al.* show a less pronounced dependence on θ_0 and are not correlated by the expression.) Plots of $\alpha_{D1}(E_0)$ are shown in Fig. 4.12 for fast neutrons normally incident on and normally reflected from concrete, soil, and iron.

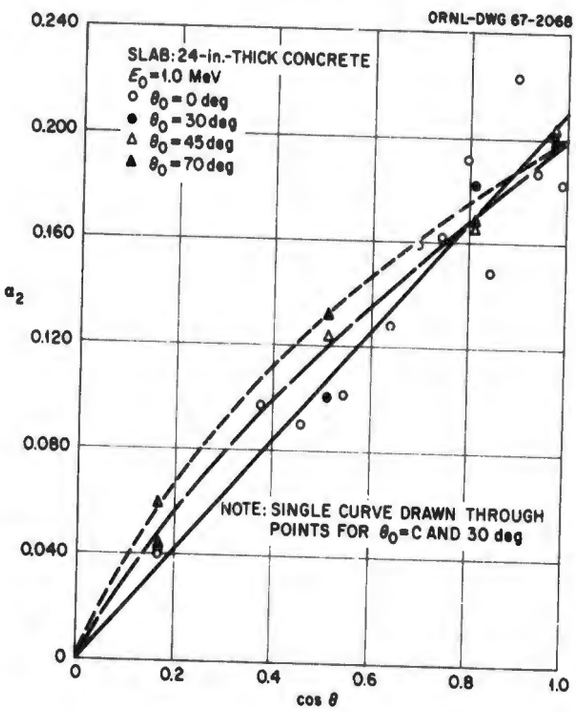

Fig. 4.11. Angular Distributions of Fast Neutrons Reflected from Concrete. (From Allen *et al.*, ref. 2.)

*The original data of Allen *et al.* were converted by French and Wells to a type 1 albedo (see Section 4.1).

Table 4.4. Values of the Constant $k(E_0)$ for the Expression Fitting the Allen *et al.* Differential Dose Albedo Data for Fast Neutrons Incident on Various Materials*

Material	$k(E_0)$ for Incident Energies of								
	0.1 MeV	0.25 MeV	0.5 MeV	1.0 MeV	2.0 MeV	3.0 MeV	5.0 MeV	14.0 MeV	Fission
Concrete	0.0948	0.1027	0.1062	0.1323	0.1164	0.1030	0.0834	0.0552	0.1110
Dry NTS soil	0.0967	0.0895	0.1002	0.1272	0.1103	0.0979	0.0784	0.0535	0.1050
50% saturated NTS soil	0.0868	0.0957	0.0952	0.1209	0.1074	0.0926	0.0746	0.0533	0.1015
100% saturated NTS soil	0.0778	0.0818	0.0839	0.1054	0.0891	0.0791	0.0644	0.0463	0.0868
Iron	0.1750	0.1752	0.1801	0.1182	0.1477	0.1508	0.1158	0.0802	0.1366

*Table taken from: R. L. French and M. B. Wells, *An Angular Dependent Albedo for Fast-Neutron Reflection Calculations*, Radiation Research Associates Report RRA-M31 (November 1963).

French and Wells found that, except for incident energies near cross-section peaks of the elements in the material, the total dose albedo data of Allen *et al.* could be correlated by a linear function of the ratio of the macroscopic hydrogen cross section of the material to its macroscopic total cross section. There is also an excellent correlation when the total albedo is averaged over the fission neutron spectrum, as is shown in Fig. 4.13 for normally incident and normally reflected fission neutrons. This correlation should be useful in extrapolating to other materials for which calculations have not been performed.

Song[5] used the Monte Carlo data of Allen *et al.* to obtain values of an energy-dependent parameter which would give the best fit to a semiempirical formula he had derived for the fast-neutron differential dose albedo for concrete. The formula,

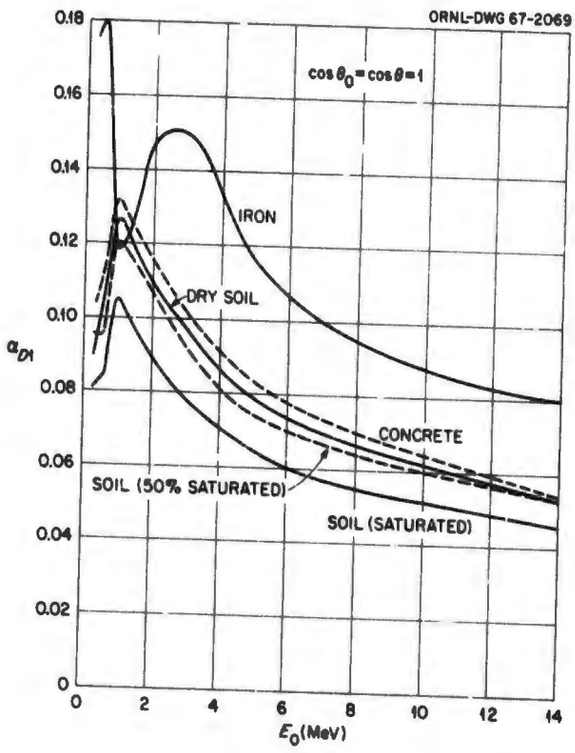

Fig. 4.12. Differential Multicollision Dose Albedo for Fast Neutrons Incident on Various Materials. (From French and Wells, ref. 4.)

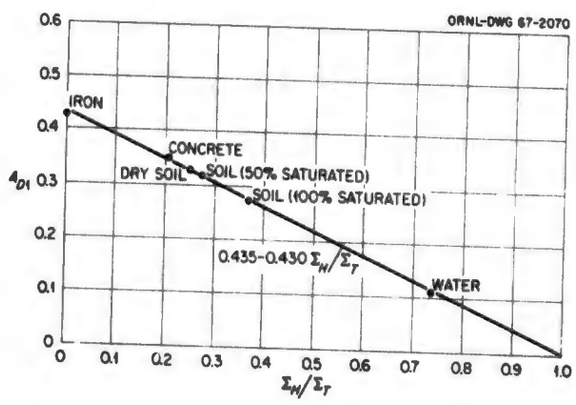

Fig. 4.13. Dependence of Fast-Neutron Total Multicollision Dose Albedo upon Hydrogen Content of Reflecting Material (Fission Neutrons, $E_0 > 0.2$ MeV). (From French and Well, ref. 4.)

derived in a manner analogous to that used by Chilton and Huddleston[6] for gamma rays, is given by

$$a_{D2}(E_0,\theta_0,\theta) = \frac{F(E_0)\cos\theta\cos\theta_0}{\cos\theta_0 + \cos\theta}, \qquad (4.16)$$

where $F(E_0)$ is the energy-dependent parameter. Song obtained values of this parameter from a least-squares analysis of the Monte Carlo data that gave the best fit to the equation. The values were then empirically correlated as a function of energy by

$$F(E_0) = E_0 \exp(0.9719 - 2.895\sqrt{E_0} + 0.3417E_0). \qquad (4.17)$$

Another investigation of fast-neutron albedos was performed by Henry, Mooney, and Provost,[7] who studied the reflection of fast neutrons normally incident on various thicknesses of steel and 6% borated polyethyethlene. Their work included both Monte Carlo calculations, with the General Dynamics SPARC code, and experiments utilizing a well-collimated reactor beam. In the experiments total dose albedos (A_{D3}) were evaluated from data obtained by traversing the beam area with a dosimeter at a position in front of the slab both with and without the slab present. As shown in Figs. 4.14 through 4.16, the experimental and calculated results are in good agreement.

The Henry *et al.* data are of particular interest in that they show the dependence of the albedo on material thickness. In addition, Fig. 4.16 shows the reduction of the steel albedo caused by facing the steel slab with various thicknesses of polyethylene. In Fig. 4.14 it appears that the albedo for steel is approaching a value of nearly 0.6, which is lower than the value of 0.84 obtained when the data of Allen *et al.* are put in the A_{D3} form. The use of a finite detector in the experiments to traverse the interface approximates the slab detector assumed in the Allen *et al.* calculations except for the low-energy cutoff, which was 0.2 MeV in the experiment and calculations performed by Henry *et al.* and was 10 eV in the calculations by Allen *et al.* When the contribution below 0.2 MeV is subtracted from the Allen *et al.* data for representative energy groups, good agreement with the results of Henry *et al.* is obtained.

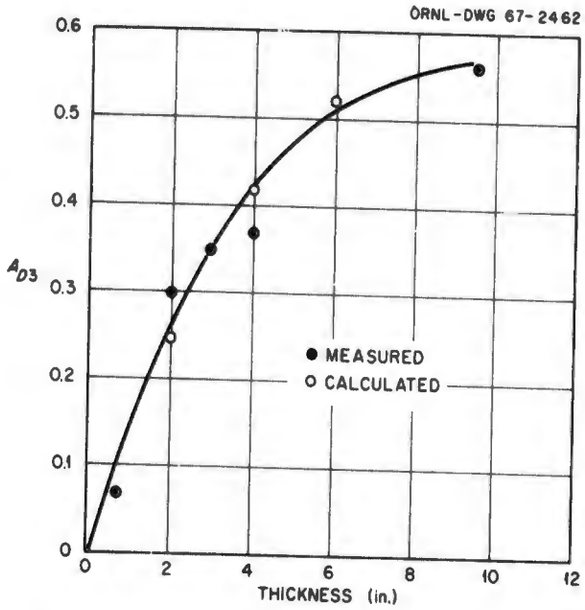

Fig. 4.14. Total Single-Collision Dose Albedos for Fission Neutrons Normally Incident on Steel Slabs: Comparison with Experiment. (From Henry, Mooney, and Provost, ref. 7.)

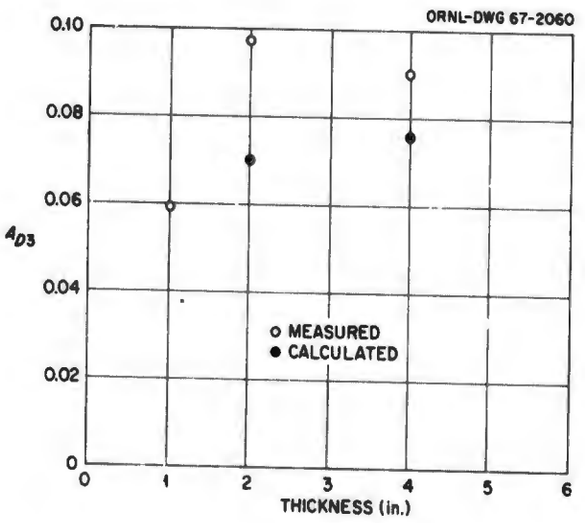

Fig. 4.15. Total Single-Collision Dose Albedos for Fission Neutrons Normally Incident on 6% Borated Polyethylene: Comparison with Experiment. (From Henry, Mooney, and Provost, ref. 7.)

From the data and discussions presented on fast-neutron albedos, it is apparent that the Monte Carlo calculations of Maerker and Muckenthaler[1] not

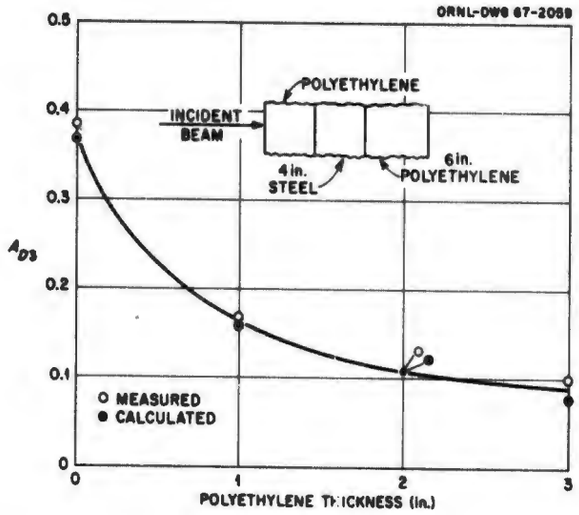

Fig. 4.16. Total Single-Collision Dose Albedos for Fission Neutrons Normally Incident on Laminated Slab of Steel and 6% Borated Polyethylene: Comparison with Experiment. (From Henry, Mooney, and Provost, ref. 7.)

only provide more detail than the other calculations but also exhibit excellent agreement with experiments. These data are recommended for obtaining the best accuracy in calculations of neutron scattering from concrete, especially for grazing angles of incidence and emergence of high-energy neutrons, where the dependence on azimuthal angle was found to be important.

For materials such as water, soil, iron, and polyethylene the Monte Carlo data of Allen *et al.*[3] are recommended. They can also be applied in calculations for concrete for those cases in which the azimuthal dependence is not important.

The highest accuracy will be obtained when the Monte Carlo data are used directly in the calculations, but the number of operations involved will virtually dictate the use of computing machines. For computer applications the albedo data may be stored in the form originally calculated and an interpolation subroutine used, or they may be calculated by a subroutine for the specific cases needed by using a fit expression. For a program to be widely applied to neutron reflection calculations, the former procedure is recommended.

If the requirements on accuracy are not too stringent, the analytical fits to the data may be applied, especially for those cases in which an azimuthal dependence is not expected to be great. The analytical fits will generally provide less information on the distribution of the scattered radiation, but they will allow the reflected dose to be computed with fewer operations. Also, the use of fit equations greatly reduces the bulk of data needed for the calculations.

If a spectrum of fast neutrons is incident on the material being considered, a more uncertain but expedient calculation may be made by using the fission spectrum albedo of Allen *et al.* shown in Fig. 4.13 with an assumed $\cos^{2/3}\theta_0 \cos\theta$ angular dependence.

4.2.2. ALBEDOS FOR NEUTRONS OF INTERMEDIATE ENERGY

The only albedos that have been obtained for neutrons whose incident and reflected energies both are in the intermediate-energy range are those calculated by Coleman, Maerker, Muckenthaler, and Stevens[8] for a steel-reinforced concrete. Using a Monte Carlo technique similar to the one used for the fast-neutron albedos,[1] they determined the distribution in energy and angle of neutrons reflected from the concrete for five incident directions and ten incident energy groups in the energy range 0.5 eV to 200 keV. The reflected distributions are given in terms of a doubly differential albedo for each of 54 different emergent directions for each energy group lying between and including the incident group and the lowest group (0.5 to 1.8 eV).

Reinforced concrete was used in these calculations because they were a part of the calculational and experimental program mentioned in Section 4.2.1. The experiment employed a 9-in.-thick concrete slab which had steel-reinforcing bars at a depth of $1\frac{1}{2}$ in. from either side; therefore all the calculations, except the fast-neutron calculations, were performed for a mock steel configuration in which each depth interval containing steel-reinforcing rods was taken as a homogenized region of concrete and steel that was 1 in. thick. The result was a five-region slab which had ordinary concrete and reinforced concrete layers of the compositions shown in Table 4.5. It was found that the effect of the iron on the neutron albedos was negligible.

Table 4.5. Compositions of Ordinary and Reinforced Concretes Used in TSF Albedo Experiments and Corresponding Monte Carlo Calculations*

(6.0 wt% H_2O; $\rho = 2.30$ g/cm^3)

Element	Composition (atoms/cm^3)	
	Ordinary Concrete	Reinforced Concrete
Hydrogen	8.50×10^{21}	8.22×10^{21}
Carbon	2.02×10^{22}	1.95×10^{22}
Oxygen	3.55×10^{22}	3.43×10^{22}
Calcium	1.11×10^{22}	1.08×10^{22}
Silicon	1.70×10^{21}	1.64×10^{21}
Magnesium	1.86×10^{21}	1.80×10^{21}
Iron	1.93×10^{20}	2.96×10^{21}
Aluminum	5.56×10^{20}	5.38×10^{20}
Potassium	4.03×10^{19}	3.95×10^{19}
Sodium	1.63×10^{19}	1.58×10^{19}

*Table taken from: R. E. Maerker and F. J. Muckenthaler, *Nucl. Sci. Eng.* **26**, 339–346 (1966).

A complete tabulation of the doubly differential albedos calculated by Coleman *et al.* is too extensive to be included here. The results, however, were numerically integrated over all exit energies to produce singly differential albedos and over all exit energies and angles to produce total albedos. The integrated results were fitted by the following expressions to within 15% for differential albedos and to within 3% for total albedos:

$$\alpha_2(\Delta E_0,\theta_0,\theta,\phi) = \frac{\mu[\epsilon_1 + \epsilon_2\mu_0 + \mu(\beta_1 + \beta_2\mu_0)]}{\mu + \gamma_1 + \gamma_2\mu_0}$$

$$\times \{1 + (1-\mu)(1-\mu_0)[a(2\cos^2\phi - 1) + b\cos\phi + c\cos^3\phi]\}, \quad (4.18)$$

and

$$A_2(\Delta E_0,\theta_0) = \delta_1 + \delta_2\mu_0, \quad (4.19)$$

where $\mu = \cos\theta$ and $\mu_0 = \cos\theta_0$, and the fit constants are given in Table 4.6 for each incident energy group. In determining the expression for the differential albedo, it was assumed that all exit neutrons had a $1/E$ energy distribution within each energy group. The expression for the total albedo was obtained by integrating Eq. 4.18 over all exit angles.

Additional calculations by Coleman *et al.*[8] yielded differential albedos for reflected thermal neutrons due to incident intermediate-energy neutrons and also effective differential albedos for "reflected" secondary gamma rays produced in the concrete as a result of the slowing down and absorption of the incident intermediate-energy neutrons. The results of these calculations are discussed in Sections 4.2.3 and 4.4.1, respectively.

4.2.3. THERMAL-NEUTRON ALBEDOS

As mentioned previously, thermal-neutron albedos can be considered as belonging to two categories: the "purely thermal" albedo, for which both the incident and the reflected neutrons are at thermal energy, and the albedo for emergent thermal neutrons that result from the moderation of neutrons that are incident at energies higher than thermal. These two categories are treated separately in the discussion below.

Neutrons Incident at Thermal Energy. – Various approximations to the purely thermal albedo have been derived analytically, with isotropic scattering and capture being the only interactions allowed. In some cases only the total albedo is derived, and it is expressed as a function of the incident angle, assuming that the reflected neutrons will emerge with isotropic or cosine distributions. In other cases differential albedos that are functions of both the incident angle and the exit angle are obtained.

In all the analytical treatments of purely thermal scattering the exit current is independent of the azimuthal angle by virtue of the isotropic-scattering assumption. Monte Carlo calculations made with the isotropic-scattering assumption have shown reasonable agreement with the other forms of analysis; however, Monte Carlo calculations in which anisotropic scattering was assumed for any hydrogen contained in a material have shown that the albedo exhibits an azimuthal dependence, although to a lesser extent than was shown for fast neutrons. Results from Monte Carlo calculations using both types of scattering assumptions

Table 4.6. Constants for the Expressions[a] Fitting the Coleman *et al.* Differential and Total Albedo Data for Intermediate-Energy Neutrons Incident on Reinforced Concrete[b]

Constant	Values of Constants for ΔE_0 of									
	55.1–200 keV	15.2–55.1 keV	4.2–15.2 keV	1.15–4.2 keV	0.32–1.15 keV	87–320 eV	24–87 eV	6.6–24 eV	1.8–6.6 eV	0.5–1.8 eV
ϵ_1	0.190	0.190	0.216	0.210	0.208	0.210	0.205	0.202	0.172	0.105
ϵ_2	−0.020	−0.025	−0.047	−0.046	−0.042	−0.061	−0.068	−0.075	−0.059	−0.036
β_1	0.020	0.025	−0.004	−0.005	−0.005	−0.003	−0.003	−0.002	0.021	0.115
β_2	0.300	0.295	0.307	0.310	0.305	0.296	0.283	0.270	0.218	0.125
γ_1	0.11	0.11	0.12	0.12	0.12	0.125	0.13	0.13	0.105	0.080
γ_2	0.91	0.91	0.91	0.91	0.91	0.865	0.845	0.82	0.65	0.48
a	0.20	0.225	0.24	0.24	0.24	0.28	0.30	0.32	0.40	0.255
b	0.56	0.69	0.70	0.70	0.70	0.72	0.73	0.74	0.77	−0.072
c	0	0	0	0	0	0	0	0	0	0.765
δ_1	0.880	0.865	0.875	0.875	0.860	0.845	0.830	0.815	0.817	0.792
δ_2	−0.208	−0.177	−0.200	−0.232	−0.205	−0.210	−0.228	−0.230	−0.244	−0.232

[a]Equations 4.18 and 4.19.

[b]Table taken from: W. A. Coleman, R. E. Maerker, F. J. Muckenthaler, and P. N. Stevens, *Nucl. Sci. Eng.* 27, 411–422 (1967).

are presented below, following the discussion of various analytical approaches.

One of the first investigations of thermal-neutron reflection was performed by Fermi,[9] who showed that for large values of N ($N = \Sigma_T/\Sigma_a$, the ratio of the total cross section to the absorption cross section) the total albedo for thermal neutrons incident on an infinitely thick, isotropically scattering medium bounded by a plane is given approximately by

$$A_2(\theta_0) = \frac{\sqrt{N} - 1}{\sqrt{N} + \sqrt{3}\cos\theta_0}, \qquad (4.20)$$

where $A_2(\theta_0)$ is the number of thermal neutrons reflected per incident thermal neutron and θ_0 is the angle of incidence.

A later, rigorous calculation was carried out by Halpern, Lueneburg, and Clark,[10] who obtained the formula

$$A_2 = \frac{1 - k}{\sqrt{N}}, \qquad (4.21)$$

where $k = 2.91$, 2.31, and 2.48 for normal, isotropic, and cosine angular distributions of incidence, respectively.

Glasstone and Edlund[11] derived a formula by use of diffusion theory which is given by

$$A_2 = \frac{1 - 2KD}{1 + 2KD}, \qquad (4.22)$$

where K is the reciprocal of the thermal-neutron diffusion length and D is the diffusion coefficient.

Chandrasekhar[12] treated radiation backscattering by a method which may in general be applied to any type of radiation that scatters isotropically with a relatively constant cross section, a condition which is approximately met by thermal-neutron scattering. The resulting backscattering angular distribution is in the form

$$a_2(\theta_0,\theta,p) = \frac{p}{2}\,\frac{\cos\theta}{\cos\theta + \cos\theta_0}$$

$$\times\, H(p,\cos\theta_0)\,H(p,\cos\theta)\,, \qquad (4.23)$$

where p is the probability of nonabsorption in a single interaction ($p = \Sigma_s/\Sigma_T$, the ratio of the scattering cross section to the total cross section) and H is a universal function tabulated[12] for various values of p and $\cos\theta_0$. The total albedo as a function of θ_0 and p is obtained by integrating Eq. 4.23 over the exit angle θ. This integration[13] yields

$$A_2(\theta_0,p) = 1 - \sqrt{1-p}\,H(p,\cos\theta_0)\,. \qquad (4.24)$$

Mockel[14] studied alternate approaches for determining the total thermal-neutron albedo for strongly absorbing media as a function of slab thickness. His motive was to develop a method that would be more readily adaptable to computer usage than the formulas of Chandrasekhar and others or the invariant embedding approach of Bellman, Kalaba, and Prestrud[15] and still provide good results with less computing time than is required for integration of the Boltzmann equation. The variational method with a constant trial function was found to give poor results except for thin slabs. In the search for better methods, three solutions were tried, which were based on an approximation to the moments of the Chandrasekhar function, a variational solution with an exponential trial function, and a diffusion-like semiempirical formula. Figures 4.17 and 4.18 compare the results from the three methods for isotropic incidence and two values of Σ_s/Σ_T. Also shown are results obtained by using a constant trial function and by numerical integration of the Boltzmann equation.

The semiempirical formula provides a fit within 2% in the case of an isotropically incident current (plane isotropic source) and within 1% for a current either normally incident or incident with a cosine distribution (isotropically incident flux). It has the form

$$A_2 = \frac{1-e^{-2\alpha x}}{1-Ae^{-2\beta x}}\left[\frac{1-f(p)}{1+f(p)} + g(p)\right], \qquad (4.25)$$

where $p = \Sigma_s/\Sigma_T$, as defined previously, and

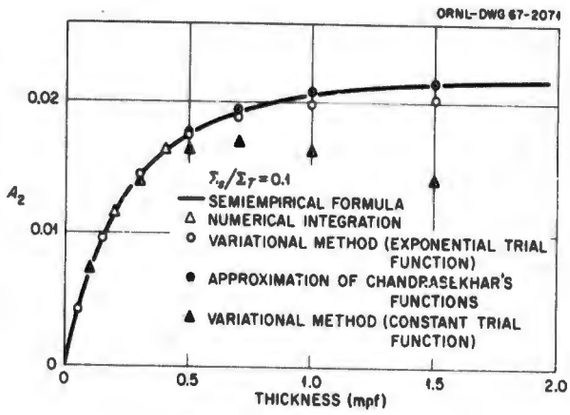

Fig. 4.17. Total Albedos Obtained by Various Methods for Thermal Neutrons Isotropically Incident on a Strongly Absorbing Medium (Σ_s/Σ_T = 0.1). (From Mockel, ref. 14.)

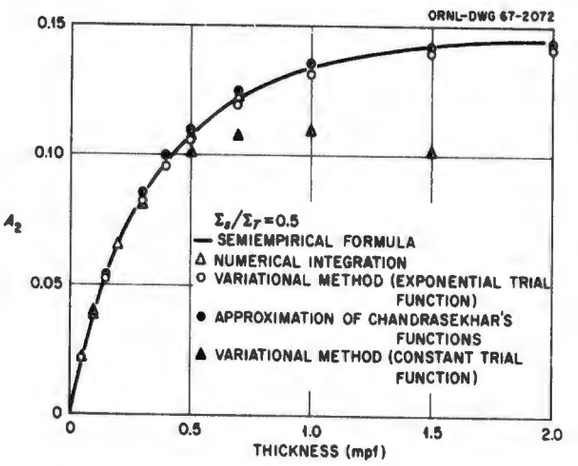

Fig. 4.18. Total Albedos Obtained by Various Methods for Thermal Neutrons Isotropically Incident on a Strongly Absorbing Medium (Σ_s/Σ_T = 0.5). (From Mockel, ref. 14.)

values of the coefficients and functions are given in Table 4.7 for three conditions of neutron incidence.

Pomraning[16] proposed a variational solution with an exponential trial function which yields for the total albedo the expression

$$A_2 = \frac{2}{(1+\nu)\ln(1-\nu^2)}\ln(1+\nu) - \nu \qquad (4.26)$$

Table 4.7. Values of Coefficients and Functions for Mockel's Semiempirical Formula (Eq. 4.25)*

Source	α	β	A	$f(p)$	$g(p)$
Normal incidence	$1.37\,(1-p)^{0.44}$	$1.37\,(1-p)^{0.44}$	0.2775	$(1-p)^{0.388}$	$0.067p^{4.46}$
Isotropic current	$1.37\,(1-p)^{0.44}$	$1.33\,(1-p)^{0.3675}$	0.640	$(1-p)^{0.5}$	0
Cosine current	$1.37\,(1-p)^{0.44}$	$1.37\,(1-p)^{0.44}$	0.3882	$(1-p)^{0.41}$	$0.05p^{3.33}$

*From: A. Mockel, *Nucl. Sci. Eng.* 22, 339 (1965).

for normally incident thermal neutrons and the expression

$$A_2 = \frac{-4}{\nu^2 \ln(1-\nu^2)} [\ln(1+\nu) - \nu]^2 \qquad (4.27)$$

for isotropically incident thermal neutrons. Here ν is a positive quantity satisfying the transcendental equation

$$\frac{2\nu}{p} = \ln\left(\frac{1+\nu}{1-\nu}\right). \qquad (4.28)$$

Values obtained with these relatively simple formulas are compared in Table 4.8 with the results of exact solutions by Chandrasekhar.[12]

Table 4.8. Comparison of Thermal-Neutron Albedos Obtained with Pomraning Formulas and with Exact Solutions of Chandrasekhar

Σ_s/Σ_T	A_2 (Normal Incidence)		Σ_s/Σ_T	A_2 (Isotropic Incidence)	
	Pomraning	Exact		Pomraning	Exact
0	0	0	0	0	0
0.25	0.046	0.045	0.10	0.020	0.022
0.35	0.071	0.070	0.20	0.043	0.046
0.45	0.100	0.098	0.30	0.071	0.074
0.55	0.136	0.135	0.40	0.104	0.107
0.65	0.183	0.180	0.50	0.144	0.147
0.75	0.246	0.248	0.60	0.192	0.195
0.85	0.342	0.340	0.70	0.254	0.257
0.95	0.538	0.536	0.80	0.340	0.342
0.98	0.672	0.673	0.90	0.477	0.478
0.99	0.753	0.753	1.0	1.0	1.0
1.0	1.0	1.0			

Equations 4.26 and 4.27 are derived from the more general expression

$$A_2 = \frac{2\Gamma}{\ln(1-\nu^2)} \ln(1+\nu) - \nu\,, \qquad (4.29)$$

where

$$\Gamma = \frac{\int_0^1 d\mu \, \frac{\mu B(\mu)}{1+\mu\nu}}{\int_0^1 \mu B(\mu)\, d\mu}\,, \qquad (4.30)$$

in which μ is the cosine of the incident angle and $B(\mu)$ is the general expression for the angular distribution of the incident flux. The success of Eqs. 4.26 and 4.27 for the cases of normal and isotropic incidence suggests that Eq. 4.29 could be applied to other angular distributions with equal success.

Wells determined total and differential thermal-neutron albedos for portland concrete[17] by analyzing Monte Carlo results obtained in a calculation that was originally performed to establish the distribution of capture gamma-ray sources in concrete and air due to thermal neutrons incident on the concrete.[18] Expressions which he derived to fit the Monte Carlo results are

$$A_1 = 0.66 \cos^{2/3}\theta_0 \qquad (4.31)$$

and

$$\alpha_1 = 0.21 \cos^{2/3}\theta_0 \cos\theta\,, \qquad (4.32)$$

which when converted to type 2 albedos are given by

$$A_2 = 0.66 \cos^{-1/3} \theta_0 \qquad (4.33)$$

and

$$\alpha_2 = 0.21 \cos^{-1/3} \theta_0 \cos \theta \, . \qquad (4.34)$$

A type 3 total albedo is obtained by integrating the differential albedo over the exit hemisphere as follows:

$$A_3(\text{port.}) = \int \alpha_1 \sec \theta \, d\Omega$$

$$= \int_0^{\pi/2} \int_0^{2\pi} 0.21 \cos^{2/3} \theta_0 \sin \theta \, d\theta \, d\phi$$

$$= 1.32 \cos^{2/3} \theta_0 \, . \qquad (4.35)$$

Expression 4.35 is to be compared with an expression obtained by Wells for a particular concrete employed in structures built at the ORNL Tower Shielding Facility:

$$A_3(\text{TSF}) = 1.3 \cos \theta_0 \, . \qquad (4.36)$$

In both of the above calculations the thermal neutrons were assumed to scatter isotropically with no energy loss, and histories were terminated after a fixed number of interactions. Statistical estimates were made for each interaction point. The concrete compositions used in these calculations are given in Table 4.9.

Table 4.9. Assumed Concrete Compositions Used in Monte Carlo Calculation by Wells*

Element	Portland Concrete (10^{21} atoms/cm^3)	TSF Concrete (10^{21} atoms/cm^3)
H	2.868	15.6
O	43.260	39.6
C	6.507	5.42
Mg		0.40
Al		1.32
Si	9.889	10.00
Ca	8.736	7.40
Fe		0.31

*M. B. Wells, *Reflection of Thermal Neutrons and Neutron-Capture Gamma Rays from Concrete*, Radiation Research Associates Report RRA-M44 (June 1966).

As part of the calculational and experimental program to investigate neutron albedos over a wide range of energies,* Maerker and Muckenthaler[19] performed single-velocity Monte Carlo calculations for a 9-in.-thick steel-reinforced concrete slab. Two different scattering laws were employed for the water contained in the concrete: (1) isotropic scattering in the laboratory system and (2) anisotropic scattering using a P_5 approximation based on experiments by Greenspan and Baksys[20] at 0.0358 eV. Scattering from all other constituents in the concrete was assumed to be isotropic in the laboratory system.

Preliminary to the calculations for the steel-reinforced concrete, the feasibility of using the Monte Carlo method for such calculations was investigated by comparing Monte Carlo results obtained for ordinary concrete with those obtained with a DTF one-energy group S_{16} calculation. A Σ_s/Σ_T value of 0.987 was used, which is typical of the ordinary concrete composition given in Table 4.5. The results for normal incidence and isotropic scattering are shown in Fig. 4.19. The excellent agreement between the two calculations

*See Sections 4.2.1 and 4.2.2 for discussions of those phases of the program in which incident fast neutrons and intermediate-energy neutrons were used. All the experiments in this program were performed at the ORNL Tower Shielding Facility.

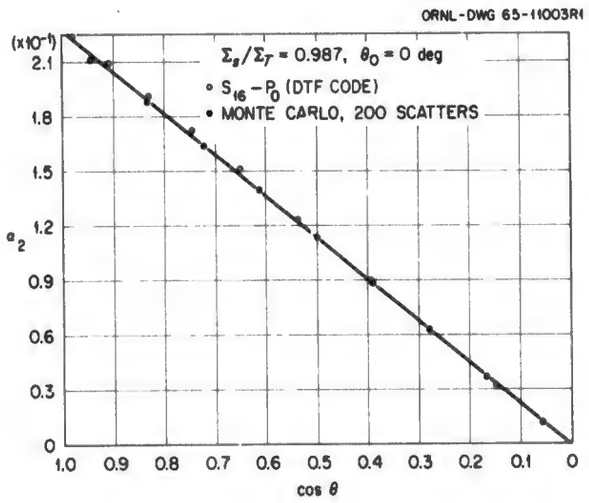

Fig. 4.19. Comparison of Differential Thermal-Neutron Albedos for Concrete Obtained with Monte Carlo and S_n Methods. (From Maerker and Muckenthaler, ref. 19.)

shows that the Monte Carlo method, which is more readily adaptable to geometric perturbations such as the steel-reinforcing bars and also to the inclusion of arbitrary anisotropic scattering functions, does give good results for this type of calculation. An investigation of the parameters limiting the calculations showed that a minimum of 50 scatterings should be used to terminate neutron histories and that a thickness of 7 mean free paths (~4 in.) reflects in excess of 95% as many neutrons as an infinitely thick slab.

As was mentioned in earlier sections of this chapter, the concrete slab used in the experimental phase of this program contained steel-reinforcing bars at a $1\frac{1}{2}$-in. depth from either side. In the calculations the slab was assumed to be divided into five homogeneous regions, the two outside regions and the middle region having a Σ_s/Σ_T value of 0.987 and the two 1-in.-thick reinforced regions having a value of 0.978. The assumed compositions for these two types of concretes are shown in Table 4.5.

Typical results from the calculations are shown in Figs. 4.20 and 4.21, both of which illustrate that the best fit to the experimental data is obtained when the scattering in water is assumed to be anisotropic. Figure 4.21 also shows that even for thermal neutrons there is some dependence of the albedo on the azimuthal angle.

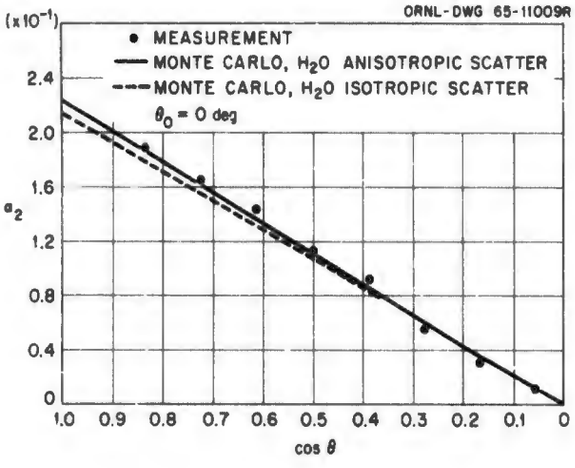

Fig. 4.20. Differential Albedos for Thermal Neutrons Normally Incident on Steel-Reinforced Concrete: Comparison of Single-Velocity Monte Carlo Calculations and ORNL TSF Experiments. (From Maerker and Muckenthaler, ref. 19.)

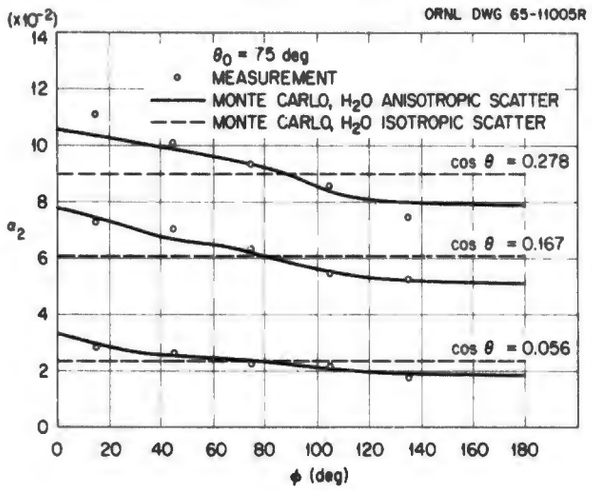

Fig. 4.21. Differential Albedos of Thermal Neutrons Incident at 75 deg on Steel-Reinforced Concrete: Comparison of Single-Velocity Monte Carlo Calculations and ORNL TSF Experiments. (From Maerker and Muckenthaler, ref. 19.)

From an analysis of their data Maerker and Muckenthaler arrived at a fitting function for the differential albedo of the form

$$\alpha_2 = \frac{0.0875\mu}{\mu + \mu_0}(1 + 1.28\mu)(1 + 1.62\mu_0 - 0.42\mu_0^2) \times [1 + (1 - \mu_0)(1 - \mu)(-0.10 + 0.43\cos\phi + 0.20\cos^2\phi)], \quad (4.37)$$

where $\mu = \cos\theta$ and $\mu_0 = \cos\theta_0$. A much simpler fit was derived for the total thermal-neutron albedo (integrated over all exit angles):

$$A_2 = 0.86 - 0.19\cos\theta_0 . \quad (4.38)$$

Results obtained for concrete using the various equations for thermal-neutron albedos are compared in Table 4.10. Comparisons are made between the total current albedo for various conditions of incidence. For all cases except $\theta_0 = 75$ deg, there would appear to be ±10% agreement between all the values. The formula due to Wells should be limited to angles of $\theta_0 < \sim 60$ deg due to its tendency to overpredict at grazing incidence.

Table 4.10. Comparison of Various Values of the Total Albedo for Thermal-Neutron Reflection from Portland Concrete*

Source	Values of A_2 Obtained by Using the Formulas of						
	Maerker and Muckenthaler	Wells	Pomraning	Halpern	Glasstone and Edlund	Fermi	Chandrasekhar
Isotropic distribution	0.78	0.792	0.8	0.719	0.74		0.79
Cosine distribution	0.734			0.698			
Monodirectional source							
$\theta_0 = 0$ deg	0.67	0.66	0.698	0.645		0.745	0.691
$\theta_0 = 45$ deg	0.72	0.74				0.78	0.730
$\theta_0 = 75$ deg	0.855	0.996				0.82	0.82

*$\Sigma_e/\Sigma_T = 0.9849$ except for Maerker-Muckenthaler results, which are based on the five-region concrete slab discussed in the text.

Neutrons Incident at Nonthermal Energies. – The only estimates available for albedos of "reflected" thermal neutrons* resulting from incident neutrons of higher energy are those from the Monte Carlo calculations of Coleman *et al.*[8] for 0.5-eV to 200-keV neutrons incident on the same steel-reinforced concrete described previously (see especially Section 4.2.2). Expressions which reproduce the Monte Carlo values to within ±15% for the differential albedos and to within ±10% for the total albedos are given in Table 4.11. The reflected angular distributions (differential albedos) for the six highest energy groups have a shape that is independent of μ_0 (the cosine of the incident poiar angle) and identical to the shape derived by Fermi[9] for the emergent angular distribution from a plane surface in the simplified case of thermal neutrons diffusing in a noncapturing and isotropically scattering semi-infinite medium.

Some contribution is also made to the emergent thermal-neutron current from the moderation of incident neutrons with energies greater than 200 keV. Coleman *et al.* accounted for these higher energy neutrons by extrapolating the results of Table 4.11 to obtain expressions for energies up to 9.57 MeV (see Table 4.12). For the spectrum of neutrons from the ORNL Tower Shielding Reactor II, which was the source used in verifying the calculations, it was estimated that a consistent error of 20% in the extrapolated results would lead to an error of only about 8% in the predicted values of the differential thermal-neutron albedos.

Figure 4.22 shows the comparison of the experimental values of $\alpha_2(\Delta E_0,\theta,\phi)$ averaged over the incident reactor spectrum with the calculated values. It can be seen from the measurements that

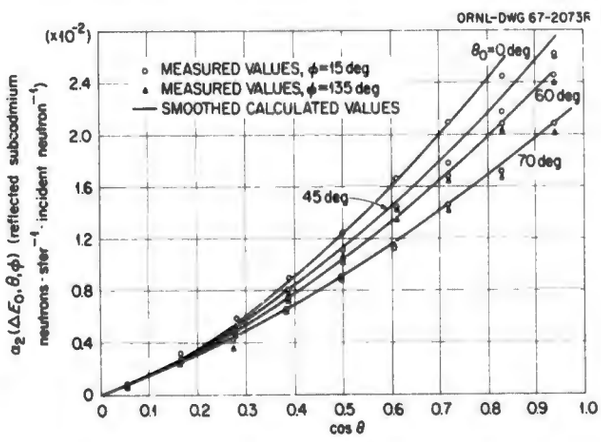

Fig. 4.22. Differential Thermal-Neutron Albedos Due to >0.5-eV Neutrons Incident on Steel-Reinforced Concrete: Comparison of Monte Carlo Calculations and ORNL TSF Experiments. (From Coleman *et al.*, ref. 8.)

*These neutrons are actually emergent neutrons produced by the slowing-down process.

the azimuthal variation of the reflected thermal neutrons is not significant, probably lying within the experimental error (~5%) except near grazing reflection. Thus the differential albedo measurements averaged over the azimuthal angle for a given μ_0 and μ could be compared with the calculated azimuthally independent values. When this was done the agreement was quite good. Of the 34 common points at which the comparisons could be made, the two largest differences are 23 and 36%. For the remaining comparisons there was a root mean square deviation of only 4.5%.

Table 4.11. Expressions for Differential and Total Thermal-Neutron Albedos Due to Incident 0.5-eV to 200-keV Neutrons[a,b]

ΔE_0	$\alpha_2(\Delta E_0,\mu_0,\mu)$ [thermal neutrons steradian^{-1} (source neutron)$^{-1}$]	$A_2(\Delta E_0,\mu_0)$ (thermal neutrons/source neutron)
55.1–200 keV	$\mu(1 + 1.73\mu)(0.0043 + 0.0058\mu_0)$	$0.029 + 0.039\mu_0$
15.2–55.1 keV	$\mu(1 + 1.73\mu)(0.0052 + 0.0059\mu_0)$	$0.035 + 0.040\mu_0$
4.2–15.2 keV	$\mu(1 + 1.73\mu)(0.0062 + 0.0071\mu_0)$	$0.042 + 0.048\mu_0$
1.15–4.2 keV	$\mu(1 + 1.73\mu)(0.0077 + 0.0073\mu_0)$	$0.052 + 0.049\mu_0$
0.32–1.15 keV	$\mu(1 + 1.73\mu)(0.0090 + 0.0099\mu_0)$	$0.061 + 0.067\mu_0$
87–320 eV	$\mu(1 + 1.73\mu)(0.011 + 0.012\mu_0)$	$0.074 + 0.081\mu_0$
24–87 eV	$\mu[(0.0185 + 0.0150\mu_0) + \mu(0.0177 + 0.0235\mu_0)]$	$0.095 + 0.096\mu_0$
6.6–24 eV	$\mu[(0.0332 + 0.0085\mu_0) + \mu(0.0220 + 0.0268\mu_0)]$	$0.150 + 0.084\mu_0$
1.8–6.6 eV	$\mu[(0.0595 + \mu(0.0290 + 0.0305\mu_0)]$	$0.248 + 0.064\mu_0$
0.5–1.8 eV	$\mu[(0.124 - 0.035\mu_0) + \mu(0.020 + 0.053\mu_0)]$	$0.431 + 0.001\mu_0$

[a]Table taken from: W. A. Coleman, R. E. Maerker, F. J. Muckenthaler, and P. N. Stevens, *Nucl. Sci. Eng.* 27, 411–422 (1967).

[b]$\mu_0 = \cos\theta_0$; $\mu = \cos\theta$.

Table 4.12. Expressions for Differential and Total Thermal-Neutron Albedos Due to Incident 200-keV to 9.57-MeV Neutrons[a,b]

ΔE_0	$\alpha_2(\Delta E_0,\mu_0,\mu)$ [thermal neutrons steradian^{-1} (source neutron)$^{-1}$]	$A_2(\Delta E_0,\mu_0)$ (thermal neutrons/source neutron)
2.64–9.57 MeV	$\mu(1 + 1.73\mu)(0.0024 + 0.0040\mu_0)$	$0.016 + 0.027\mu_0$
0.750–2.64 MeV	$\mu(1 + 1.73\mu)(0.0028 + 0.0044\mu_0)$	$0.019 + 0.030\mu_0$
200–750 keV	$\mu(1 + 1.73\mu)(0.0036 + 0.0049\mu_0)$	$0.024 + 0.033\mu_0$

[a]Table taken from: W. A. Coleman, R. E. Maerker, F. J. Muckenthaler, and P. N. Stevens, *Nucl. Sci. Eng.* 27, 411–422 (1967).

[b]$\mu_0 = \cos\theta_0$; $\mu = \cos\theta$.

4.3 Gamma-Ray Albedos

The primary interaction which contributes to the backscattering or material albedo of gamma rays is Compton scattering from electrons. In this interaction the photon rebounds with an energy which is directly dependent on the scattering angle and the incident energy, and is given by the Klein-Nishina formula.[21] The higher the incident energy the more strongly will the forward direction be favored. Thus the gamma-ray albedo has an inverse relationship with the incident photon energy. Due to the strongly peaked forward scattering, the gamma-ray albedo also has a strong dependence on the azimuthal angle ϕ. That is, the scattering angle θ_s (see Fig. 4.1) at $\phi = 0$ deg is smaller than the scattering angle at $\phi = 180$ deg, and hence the albedo decreases with increasing ϕ. The magnitude of the difference increases with increasing values of the incident polar angle θ_0, so that at grazing incidence the difference lies between forward scattering ($\phi = 0$ deg) and backscattering ($\phi = 180$ deg).

Another interaction which contributes to the "reflected energy" for incident gamma rays of high energy is pair production. The positron created in this reaction is annihilated by combination with an atomic electron, releasing energy in the form of two new gamma rays. This reaction is possible only if the energy of the incoming gamma ray is greater than 1.022 MeV, and it is predominant only at energies above about 5 MeV. The photons that are created each have an energy of 0.511 MeV, which is greater than the maximum energy possible for gamma rays scattered backward ($\theta_s = 180$ deg) by Compton scattering.

Leimdorfer[22] investigated the relative contributions by positron annihilation and Compton scattering to the total gamma-ray albedo for concrete in a calculation which considered single scatterings only. The results for normally incident gamma rays are shown in Fig. 4.23, in which the fraction of the albedo due to annihilation is plotted as a function of the incident gamma-ray energy. Also plotted is the same fraction from a calculation by Wells[23] in which multiple scatterings were considered.

Most of the studies of gamma-ray albedos have been carried out either by Monte Carlo analysis or by experiments, and, as was the case for neutrons, most of them have been for concrete. For those cases for which both experimental and calculated data are available, there is good agreement; however, experiments have been limited to low gamma-ray energies which can be obtained from isotope sources, and definitive Monte Carlo calculations have been performed for only a few materials.

One of the earliest Monte Carlo calculations was performed by Berger and Doggett,[24] who obtained the total dose albedo A_{D3} for monoenergetic sources incident on iron, tin, lead, and water. From these calculations was obtained a quantitative measure of the dependence of the albedo on the thickness of the scattering material. This dependence is illustrated for iron and water in Table 4.13.

Berger and Raso[25,26] carried out an extensive series of Monte Carlo calculations to determine the total energy albedo for monoenergetic gamma rays incident on a variety of materials, and in some cases obtained energy and angular distri-

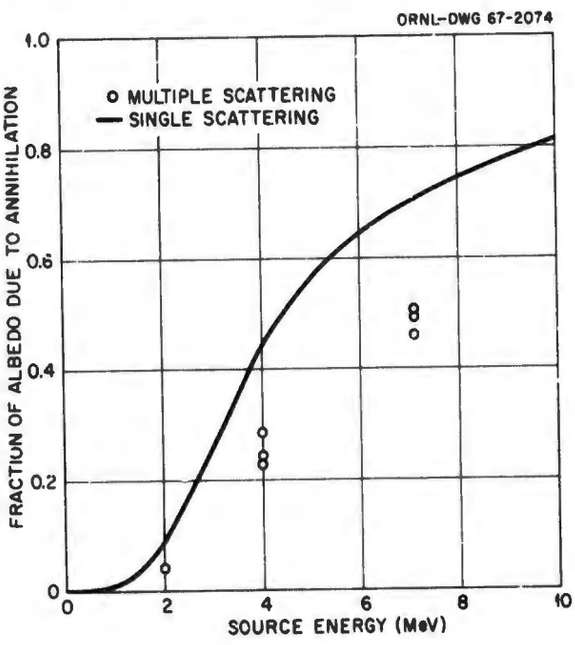

Fig. 4.23. Ratio of Pair Production Annihilation Albedo to Total Albedo for Gamma Rays Normally Incident on Concrete. (From Leimdorfer, ref. 22, and Wells, ref. 23.)

Table 4.13. Dependence of Gamma-Ray Total Dose Albedo (A_{D3}) on Material Thickness*

Material	E_0 (MeV)	θ_0 (deg)	Fraction of Reflected Photons Reflected Within Depth of		
			0.5 mfp	1.0 mfp	2.0 mfp
H_2O	0.66	0	0.65	0.88	0.99
	0.66	60	0.61	0.96	1.0
Fe	1.0	0	0.79	0.93	1.0
	1.0	60	0.89	0.98	1.0

*Table taken from: J. M. Berger and J. Doggett, *J. Res. Natl. Bur. Std.* 56, 89 (1956).

butions. An interesting result of their work is the analysis of the variation in the total albedo with the atomic number of the scattering material. Plots of the albedo for normally incident gamma rays are shown in Fig. 4.24. These data may be fitted by relatively smooth curves; however, data at intermediate Z values would greatly increase confidence in the fits, particularly for the 2.0-MeV cases.

Raso[27] performed additional calculations for concrete for source energies of 0.5, 1, 2, 4, 6, and 10 MeV and polar angles of incidence of cos θ_0 = 0.10, 0.25, 0.50, 0.75, and 1.0. The emergent gamma rays were divided into 8 polar and 12 azimuthal angular increments, and differential dose albedos $\alpha_{D2}(E_0,\theta_0,\theta,\phi)$ were obtained for all exit angle combinations. Total albedos $A_{D2}(E_0,\theta_0)$ were obtained for each incident energy and angle. Values of the differential and total dose albedos for normal incidence are shown in Figs. 4.25 and 4.26 respectively.

Figures 4.25 and 4.26 also show Monte Carlo results obtained by Wells,[23] who calculated differential and total dose albedos for gamma-ray reflection from concrete by analysis of prior Monte Carlo data[28] on gamma-ray scattering in air and concrete. The results of Raso and Wells are essentially in good agreement on the total albedo for energies of 2 MeV and below, although there are some differences in the differential albedos at these energies. At energies above 2 MeV there is a substantial disagreement between Raso and Wells on the magnitude of the total albedo, as

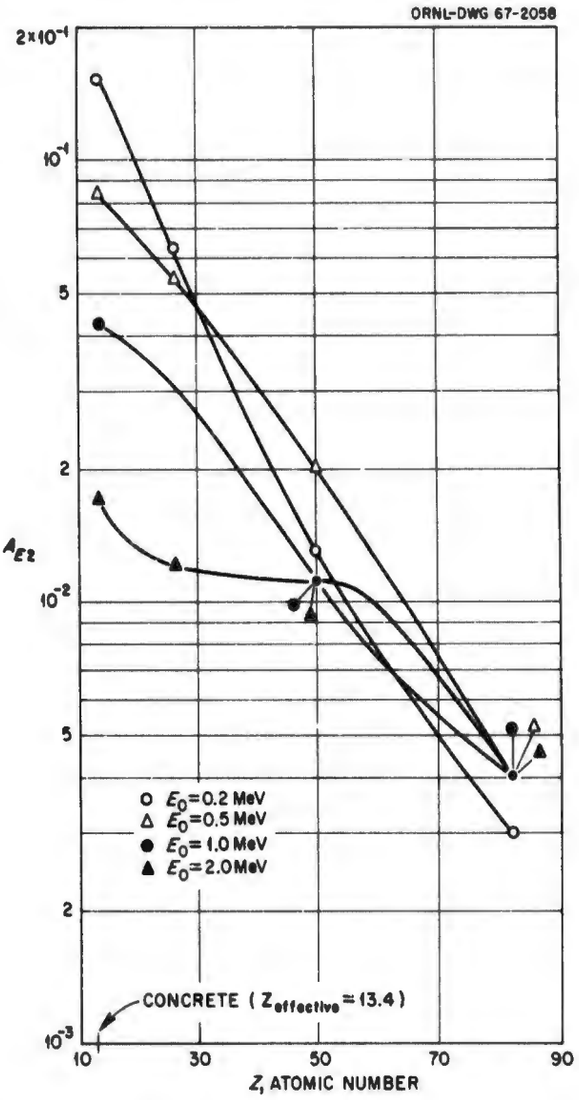

Fig. 4.24. Total Energy Albedo for Normally Incident Monoenergetic Gamma Rays as a Function of the Atomic Number of the Material. (From Berger and Raso, refs. 25 and 26.)

shown in Fig. 4.26. The divergence of agreement with increasing energy could be attributed to the different manner in which pair production was treated in the two calculations.

As is apparent from Fig. 4.25, the incident energies used in the Wells calculations were 0.6, 1, 2, 4, and 7 MeV. The incident polar angles were 0, 30, 45, 60, and 75 deg. The emergent angles varied with the individual problems and no regularly spaced grid was used, but by extrapolation and interpolation, smooth curve fits were

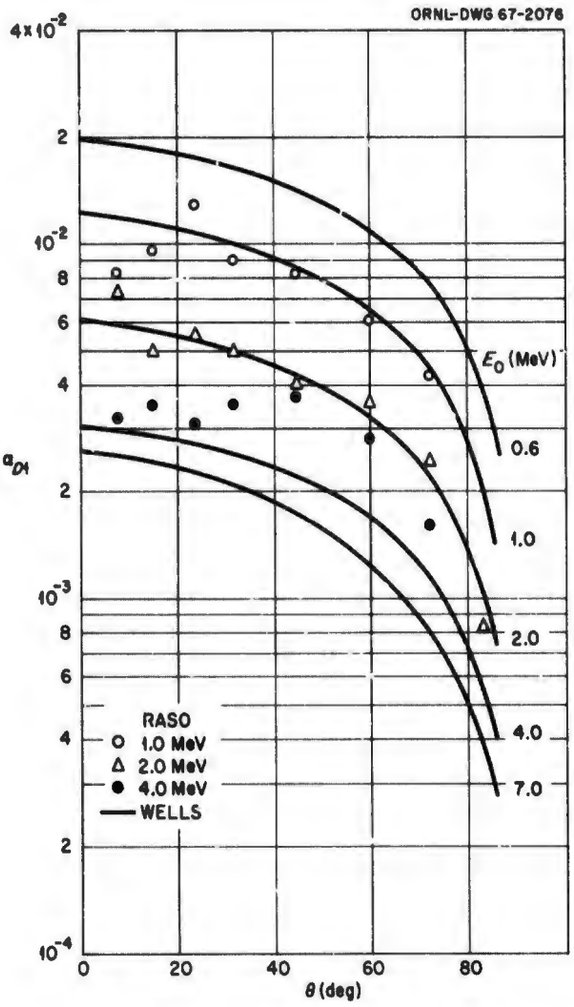

Fig. 4.25. Differential Dose Albedos for Gamma Rays Normally Incident on Concrete. (From Wells, ref. 23, and Raso, ref. 27.)

obtained for a_{D1} vs θ for azimuthal angles of 0 and 180 deg. The results for $\theta_0 = 30$ deg are given in Figs. 4.27 and 4.28, for $\theta_0 = 45$ deg in Figs. 4.29 and 4.30, for $\theta_0 = 60$ deg in Figs. 4.31 and 4.32, and for $\theta_0 = 75$ deg in Figs. 4.33 and 4.34. Extrapolation to other values of ϕ may be effected by using Eq. 4.42 and the trigonometric identity $\cos\theta_s = \sin\theta_0 \sin\theta \cos\phi - \cos\theta_0 \cos\theta$..

Chilton and Huddleston[6] developed a semiempirical formula for the differential dose albedo for concrete of the form

$$a_{D2}(E_0,\theta_0,\theta,\phi) = \frac{CK(\theta_s) \times 10^{26} + C'}{1 + [(\cos\theta_0)/(\cos\theta)]}, \tag{4.39}$$

where $K(\theta_s)$ is the Klein-Nishina differential energy scattering coefficient for the scattering angle θ_s, and C and C' are adjustable parameters dependent on the initial energy. Values of $K(\theta_s)$ are given in ref. 9. The most accurate values of C and C' were obtained by Chilton, Davisson, and Beach[29] from an analysis of earlier Monte Carlo calculations performed by Davisson and Beach.[30] Fit parameters were obtained by normalization to the total calculated albedo rather than to the differential data. The resulting values of C and C' are given in Table 4.14 for water, concrete, iron, and lead.

Chilton[31] also devised a fit to type 2 differential albedo data obtained by Berger and Morris[32] in Monte Carlo calculations for a semi-infinite concrete slab and gamma rays from ^{60}Co (1.25 MeV)

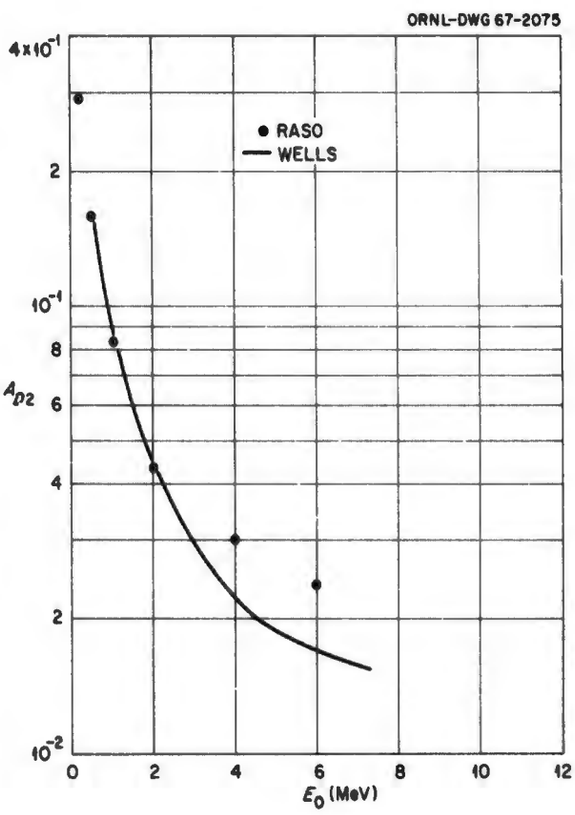

Fig. 4.26. Total Dose Albedos for Gamma Rays Normally Incident on Concrete. (From Wells, ref. 23, and Raso, ref. 27.)

Table 4.14. Values of Parameters for Chilton-Huddleston Gamma-Ray Differential Albedo Formula (Eq. 4.39)*

Material	E_0 (MeV)	C	C'
Water	0.2	−0.0187 ± 0.0027	0.1327 ± 0.0054
	0.662	0.0309 ± 0.0047	0.0253 ± 0.0034
	1.00	0.0470 ± 0.0053	0.0151 ± 0.0025
	2.50	0.0995 ± 0.0068	0.0058 ± 0.0010
	6.13	0.1861 ± 0.0107	0.0035 ± 0.0005
Concrete	0.2	0.0023 ± 0.0033	0.0737 ± 0.0065
	0.662	0.0347 ± 0.0050	0.0197 ± 0.0035
	1.00	0.0503 ± 0.0056	0.0118 ± 0.0025
	2.50	0.0999 ± 0.0078	0.0051 ± 0.0011
	6.13	0.1717 ± 0.0103	0.0048 ± 0.0005
Iron	0.2	0.0272 ± 0.0033	−0.0100 ± 0.0062
	0.662	0.0430 ± 0.0045	0.0063 ± 0.0030
	1.00	0.0555 ± 0.0049	0.0045 ± 0.0021
	2.50	0.1009 ± 0.0073	0.0044 ± 0.0010
	6.13	0.1447 ± 0.0101	0.0077 ± 0.0006
Lead	0.2	0.0044 ± 0.0002	−0.0050 ± 0.0004
	0.662	0.0308 ± 0.0015	−0.0100 ± 0.0007
	1.00	0.0452 ± 0.0013	−0.0083 ± 0.0004
	2.50	0.0882 ± 0.0014	0.0001 ± 0.0002
	6.13	0.1126 ± 0.0048	0.0063 ± 0.0003

*Table taken from: A. B. Chilton, C. M. Davisson, and L. A. Beach, *Trans. Am. Nucl. Soc.* 8, 656 (1965).

and ^{137}Cs (0.662 MeV). This fit is of the form

$$\alpha_{D2}(\theta_0,\theta,\phi) = B(\theta_0,\theta,\phi) \times \frac{CK(E_0,\theta_s) \times 10^{26} + C'}{1 + \cos\theta_0 \sec\theta[1 + 2E_0(1 - \cos\theta_s)]^{1/2}}, \quad (4.40)$$

where $K(E_0,\theta_s)$ is again the Klein-Nishina differential energy scattering coefficient,

$$B(\theta_0,\theta,\phi) = M_1 + M_2(1 - \cos\theta_0)^2 + M_3(1 - \cos\theta)^2 + M_4(1 - \cos\theta_0)^2(1 - \cos\theta)^2 + M_5(1 - \cos\theta_0)(1 - \cos\theta)(1 - \cos\phi), \quad (4.41)$$

and values of the constants for the two initial energies are given in Table 4.15. The fit to the Monte Carlo data is good to the order of 2 to 6%.

In most of the experimental studies of gamma-ray albedos the sources used were ^{60}Co and ^{137}Cs. Examples are the data obtained for concrete by Clifford,[33] Haggmark *et al.*,[34] and Barrett and Waldman.[35] Comparisons of typical data from these investigations with results from some of the calculations discussed previously are shown in Figs. 4.35 through 4.39. For these figures all the values were converted to type 1 albedos, and, where necessary, the analytical data were interpolated to match the experimental energies.

Except for small angles of reflection, the experimental and calculated values shown in Figs. 4.35 through 4.39 are all in good agreement. In particular, the Wells calculations agree with nearly all the experimental values, deviating most from the data of Clifford. As is demonstrated by Figs. 4.35, 4.36, and 4.37, the agreement between the Wells calculations and the data of Haggmark *et al.* is especially close, even for small angles of reflection. Figure 4.38 shows that there is also good agreement between the calculations of Wells and the data of Barrett and Waldman except near normal reflection (θ = 0 deg). For those cases which can be compared, the calculations of Berger and Morris and values obtained with the Chilton-Huddleston formula are also in good agreement with the experimental data, and give the closest

Table 4.15. Values of Parameters for Chilton's Fit (Eq. 4.40) to Monte Carlo Gamma-Ray Differential Albedo Data*

Parameter	^{137}Cs Source (0.662 MeV)	^{60}Co Source (1.25 MeV)
C	0.0455	0.0710
C'	0.0161	0.0114
M_1	1.512	1.555
M_2	−0.606	−0.629
M_3	−0.641	−0.605
M_4	0.645	0.539
M_5	−0.157	−0.168

*Table taken from: A. B. Chilton, *Trans. Am. Nucl. Soc.* 9, 369 (1966).

agreement with the Clifford data. For the single case shown (Fig. 4.36), the weighted values of Raso and the Wells calculations are very similar. Both Fig. 4.37 and Fig. 4.39 point up the strong dependence on ϕ for obliquely incident radiation.

Haggmark *et al.*[34] found that their data on differential dose albedos for concrete and also for iron and aluminum could all be represented by the expression

$$\alpha_{D3}(E_0,\theta_0,\theta_s) - b = e^{-\pi\theta_s}, \qquad (4.42)$$

where θ_s is the scattering angle described previously (see Fig. 4.1); α_{D3} is the differential dose albedo described in Section 4.1 except that the exit direction is expressed in terms of θ_s, which is a function of θ and ϕ; and b is an empirical constant for a given θ_0, E_0, and material. Figure 4.40 shows a comparison of Eq. 4.42 with the experimental data for iron, concrete, and aluminum reduced by the appropriate b value given in Table 4.16. A plot of the differential albedo for concrete obtained with an equation of the same form as Eq. 4.42 is compared with the data of Clifford in Fig. 4.41 for the case of ^{137}Cs gamma rays incident at cos θ_0 = 0.5. The coefficients used in the equation shown in the figure gave a slightly better fit to these particular data than Eq. 4.42, which, however, has more general applicability. The same plot is compared with values calculated with the Chilton-Huddleston formula (Eq. 4.39) in Fig. 4.42. (Note: Equation 4.42 is a useful tool for extrapolating the albedo data of Wells presented in Figs. 4.28 through 4.34 to values of the azimuthal angle ϕ other than 0 and 180 deg.)

An experiment was performed by Clarke and Batter[36] to measure the effect of extended concrete surfaces on the dose from a point source. As shown in Fig. 4.43*a*, the detector and source were maintained at the same level, whereas both the source-detector separation distance and the height above the concrete surface were varied. The sources used were ^{60}Co and ^{192}Ir. The variation in dose was found to be a smooth function of the ratio of the height h to the separation distance d which did not vary significantly with changes in the separation distance when the height was varied to maintain a constant value of the ratio. This is demonstrated in Fig. 4.43*b*, which shows the percent increase in the dose from the ^{192}Ir source due to scattering from the concrete,

Table 4.16. Values of the Constant b Fitting the Expression of Haggmark *et al.* (Eq. 4.42) for Gamma-Ray Differential Dose Albedos for Al, Fe, and Concrete*

Material	Source	cos θ_0	b
Al	^{60}Co	0.50	0.0070
		0.75	0.0090
		1.00	0.0095
	^{137}Cs	0.50	0.0132
		0.75	0.0167
		1.00	0.0194
Fe	^{60}Co	0.50	0.0060
		0.75	0.0065
		1.00	0.0065
	^{137}Cs	0.50	0.0091
		0.75	0.0120
		1.00	0.0130
Concrete	^{60}Co	0.50	0.0075
		0.75	0.0090
		1.00	0.0100
	^{137}Cs	0.50	0.0133
		0.75	0.0165
		1.00	0.0184

*Table taken from: L. G. Haggmark *et al.*, *Nucl. Sci. Eng.* 23, 138 (1965).

and in Fig. 4.43*c*, which shows the ratio of the dose rate from the ^{60}Co source that is scattered from the concrete to the direct dose rate. [The ^{60}Co data for a height of 9 ft is from the work of Jones *et al.* (Convair report CVAC-170).[37]]

Figure 4.43*c* also shows the results obtained by Clarke and Batter with the Chilton-Huddleston differential dose albedo formula. Although preliminary values of the constants C and C' were used for this calculation, the agreement with the experimental data is good. Later calculations by Chilton[38] with improved values of the constants (those given in Table 4.14) also correlate well with the experimental data. On the basis of Chilton's work, which included the case in which the source and detector positions were allowed to vary independently, it was found that the best fit to the experimental data is obtained when it is assumed that all reflections occur at a depth of 1.7 cm in the material and the albedo formula

is integrated over a plane at that depth. Obviously this correction to the location of the interface would be important only when the source or detector or both are near the interface.

Measurements similar to those of Clarke and Batter were made by Hendee and Ellis[39] except that a shadow shield was placed between the source and detector and measurements were made for unequal source and detector heights as well as for equal heights. The sources used were ^{60}Co and ^{137}Cs, and the scattering surfaces were lead, concrete, and water. The results indicate that the ratio of the average height of the source and detector to the distance between the source and detector is the parameter most influential in determining the dose scattered from the slabs. For the cases considered, no significant influence on the scattered dose was observed by positioning the source at a height greater or lesser than that of the detector. For h/d values greater than 0.5, curves closely fitting the experimental points were obtained from calculations in which isotropic energy albedos (α_{E2}) were used. In the case of the ^{60}Co source these values were 0.050, 0.0113, and 0.049 for concrete, lead, and water respectively. The corresponding values for the ^{137}Cs source are 0.100, 0.013, and 0.083. For h/d values less than 0.5 the reflection curves calculated with the isotropic albedos were below the experimental values.

Some measurements of the spectra of gamma rays scattered from a variety of materials were carried out by Andrews and Steyn,[40] but a complete listing of their data is not available. In the sample results published in ref. 40 peaks due to single and double scatterings are clearly visible.

In a theoretical approach Eisenhauer[41] used an image source technique to study the problem of radiation reflection from a point source located above a surface. It was shown that the geometrical effects can be taken into account by a simple scaling function. For a given material and radiation the remaining effects depend primarily on one angular variable, with only a secondary dependence on the ratio of the source height to the detector height. Some applications were made to neutrons, gamma rays, and particles whose energy does not change with scattering (one-velocity case).

Leimdorfer used the Monte Carlo method to calculate the total gamma-ray energy flux albedo from concrete slabs[22] and also from spherically concave concrete walls.[42] An interesting result of the latter studies is shown in Fig. 4.44, which gives the energy flux albedo A_{E3} for 1-MeV gamma rays from a concrete wall surrounding a spherical cavity as a function of the radius of curvature of the wall. The point isotropic source is located in the center of an evacuated cavity in an infinite concrete medium. The energy flux albedo A_{E3} is defined as the ratio of the collided to the uncollided energy flux at the wall surface. The infinite radius (flat surface) albedo is calculated to be only about 2.5% higher than the albedo for a 500-cm-radius spherical cavity. Other interesting conclusions drawn by Leimdorfer from these calculations are that reflections beyond the third or fourth order do not contribute appreciably to the energy flux albedo in the spherical geometry and that at least 90% of the reflections occur within the first 24-g/cm^2 thickness for gamma-ray energies below 10 MeV.

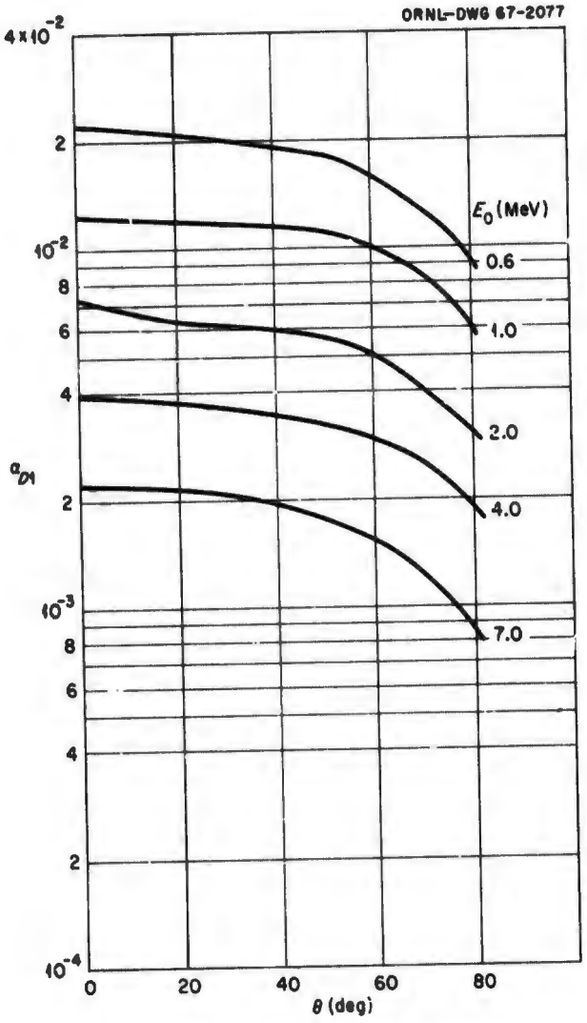

Fig. 4.27. Differential Dose Albedos for Gamma Rays Incident on Concrete at 30 deg (ϕ = 0 deg). (From Wells, ref. 23.)

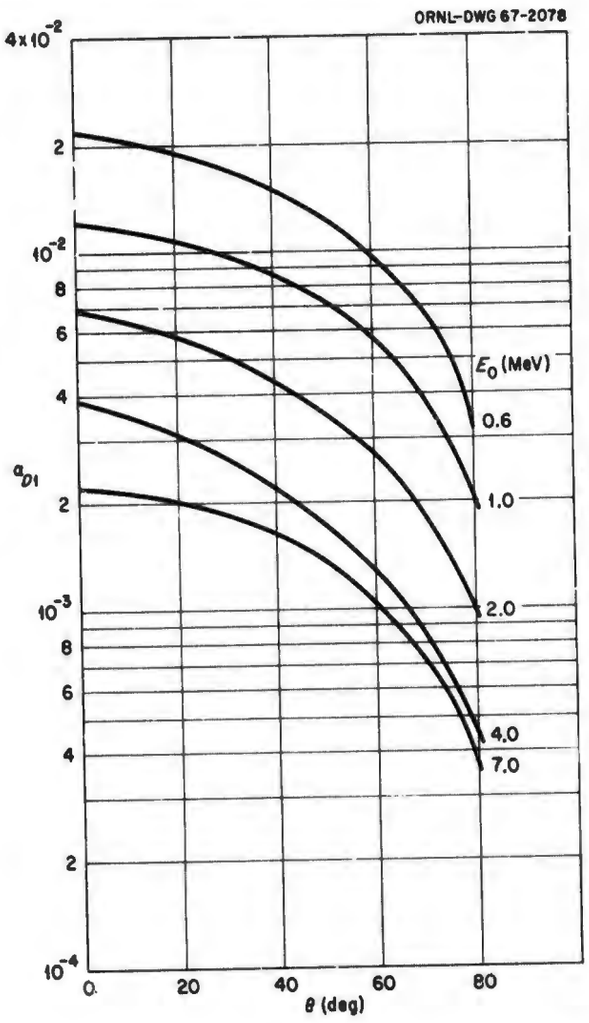

Fig. 4.28. Differential Dose Albedos for Gamma Rays Incident on Concrete at 30 deg (ϕ = 180 deg). (From Wells, ref. 23.)

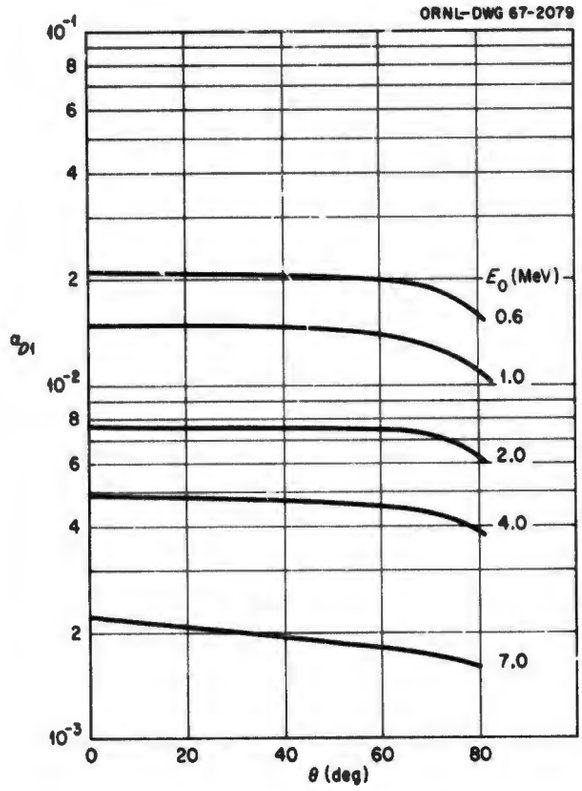

Fig. 4.29. Differential Dose Albedos for Gamma Rays Incident on Concrete at 45 deg (ϕ = 0 deg). (From Wells, ref. 23.)

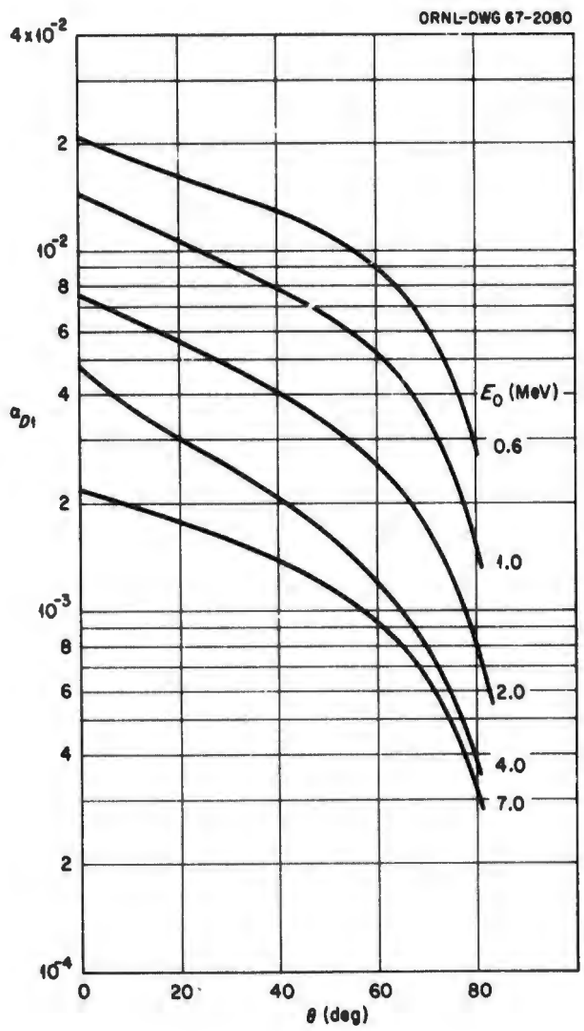

Fig. 4.30. Differential Dose Albedos for Gamma Rays Incident on Concrete at 45 deg (ϕ = 180 deg). (From Wells, ref. 23.)

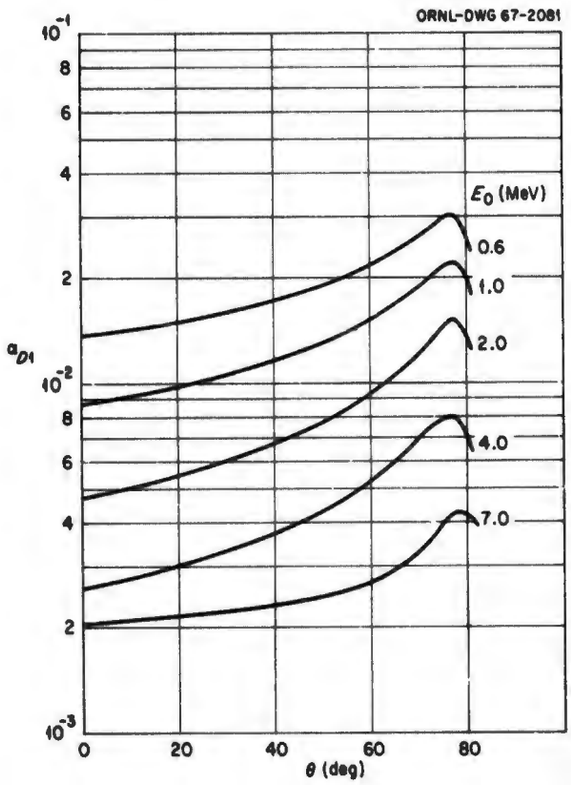

Fig. 4.31. Differential Dose Albedos for Gamma Rays Incident on Concrete at 60 deg (ϕ = 0 deg). (From Wells, ref. 23.)

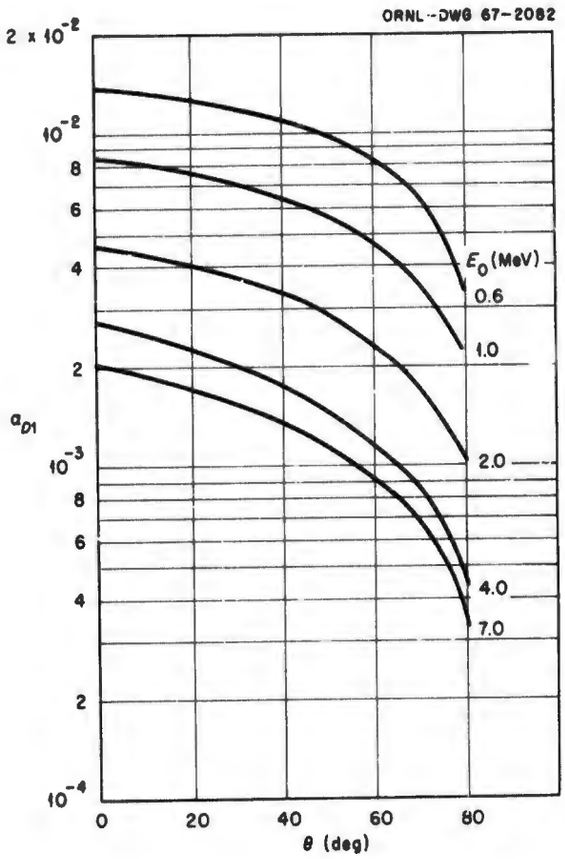

Fig. 4.32. Differential Dose Albedos for Gamma Rays Incident on Concrete at 60 deg (ϕ = 180 deg). (From Wells, ref. 23.)

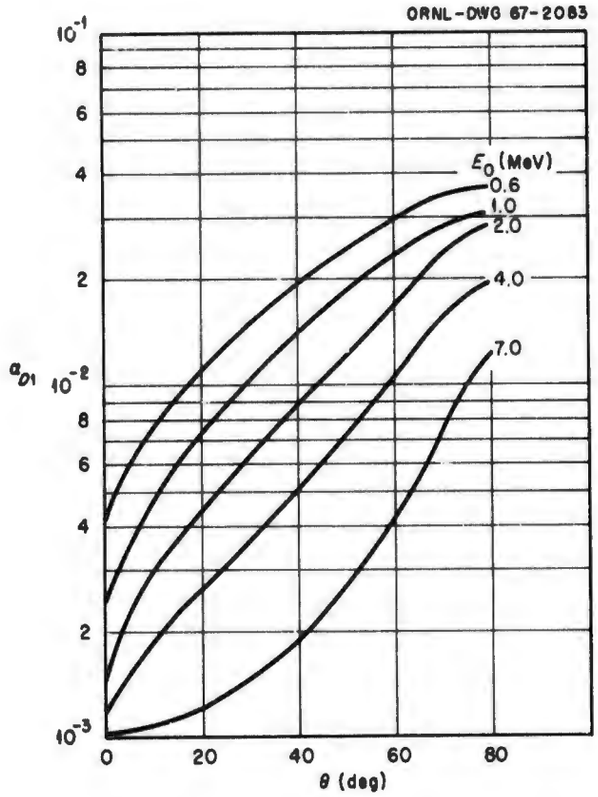

Fig. 4.33. Differential Dose Albedos for Gamma Rays Incident on Concrete at 75 deg (ϕ = 0 deg). (From Wells, ref. 23.)

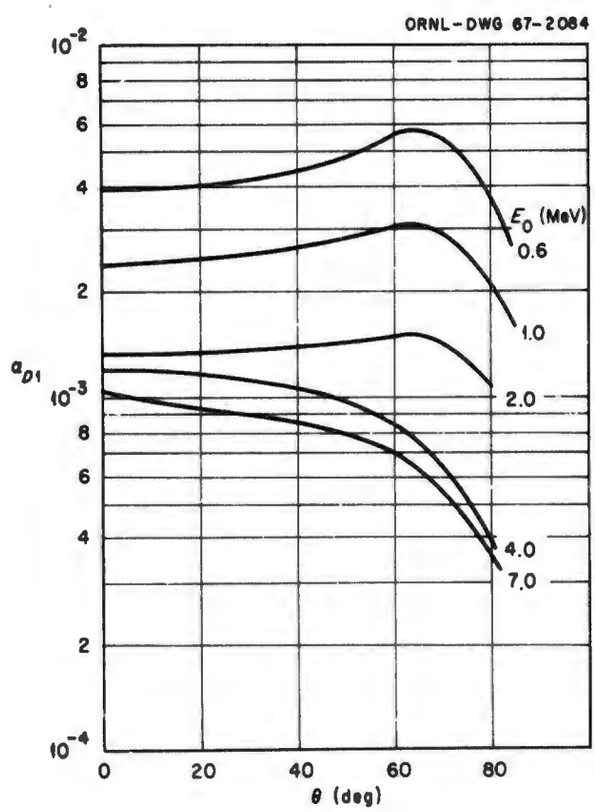

Fig. 4.34. Differential Dose Albedos for Gamma Rays Incident on Concrete at 75 deg (ϕ = 180 deg). (From Wells, ref. 23.)

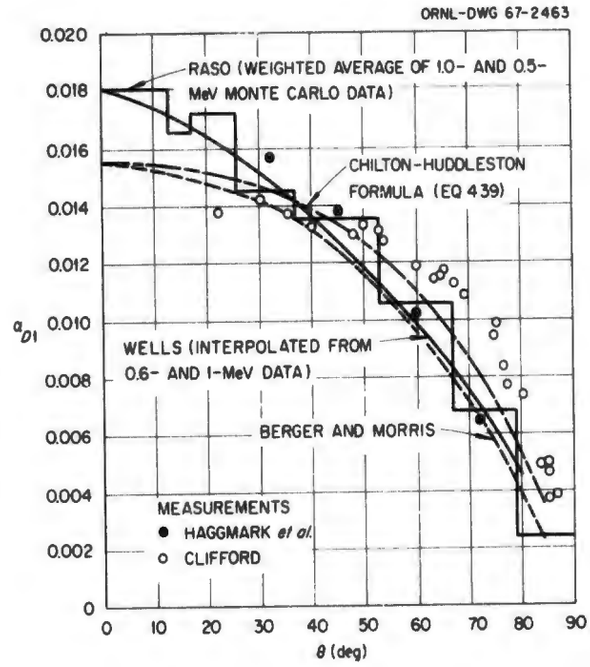

Fig. 4.36. Comparison Between Calculated and Measured Differential Dose Albedos for ^{137}Cs Gamma Rays (0.662 MeV) Normally Incident on Concrete. (From Wells, ref. 23.)

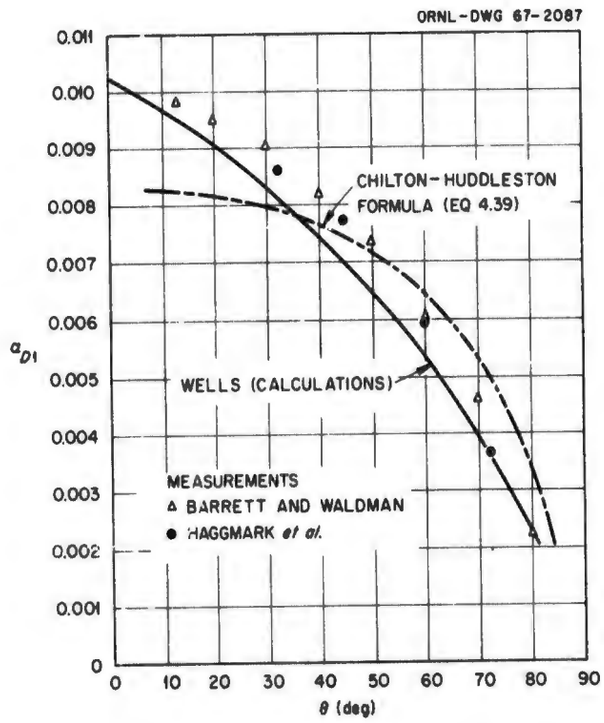

Fig. 4.35. Comparison Between Calculated and Measured Differential Dose Albedos for ^{60}Co Gamma Rays (1.25 MeV) Normally Incident on Concrete. (From Wells, ref. 23.)

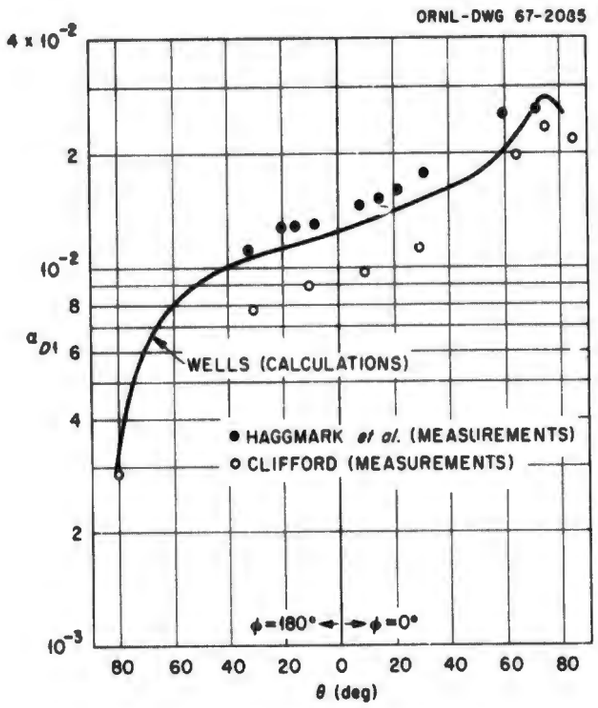

Fig. 4.37. Comparison Between Calculated and Measured Differential Dose Albedos for ^{137}Cs Gamma Rays (0.662 MeV) Incident on Concrete at 60 deg. (From Wells, ref. 23.)

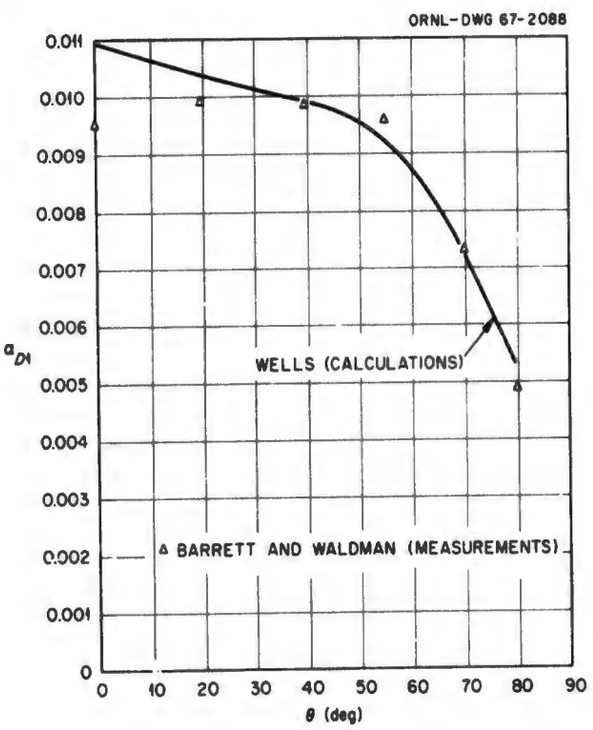

Fig. 4.38. Comparison Between Calculated and Measured Differential Dose Albedos for ^{60}Co Gamma Rays (1.25 MeV) Incident on Concrete at 30 deg (ϕ = 0 deg). (From Wells, ref. 23.)

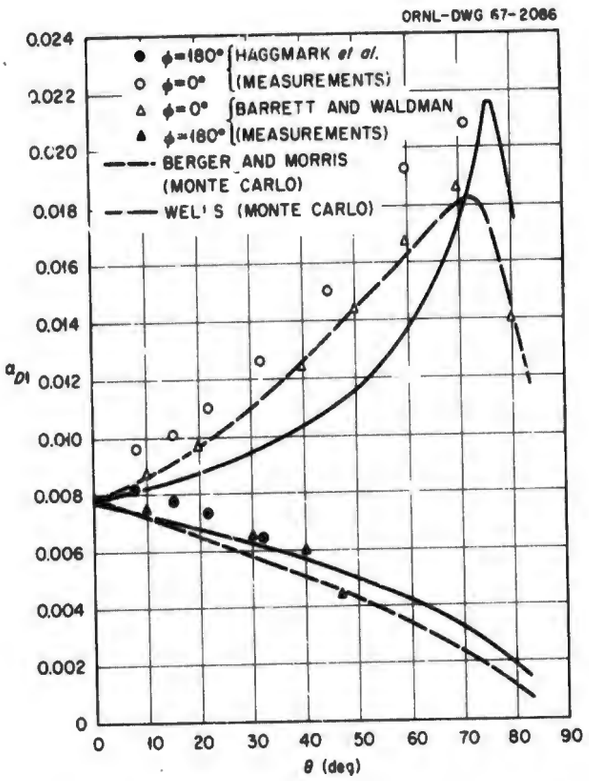

Fig. 4.39. Comparison Between Calculated and Measured Differential Dose Albedos for ^{60}Co Gamma Rays (1.25 MeV) Incident on Concrete at 60 deg. (From Wells, ref. 23.)

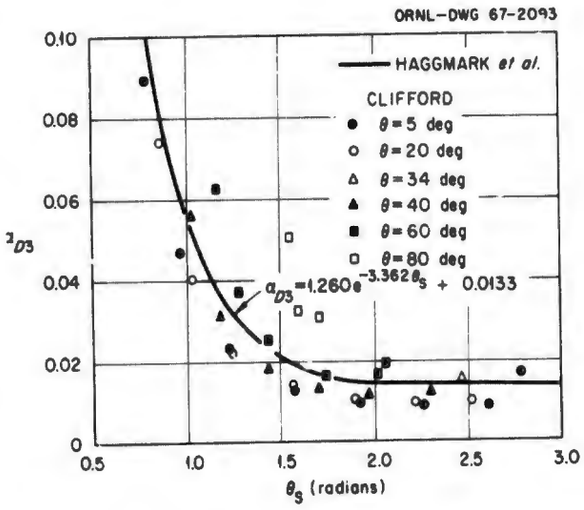

Fig. 4.41. Comparison of Gamma-Ray Differential Dose Albedos for Concrete Obtained with Equation 4.42 with Experimental Data of Clifford. ^{137}Cs gamma rays (0.662 MeV) incident on concrete at cos θ_0 = 0.5. (From Haggmark *et al.*, ref. 34.)

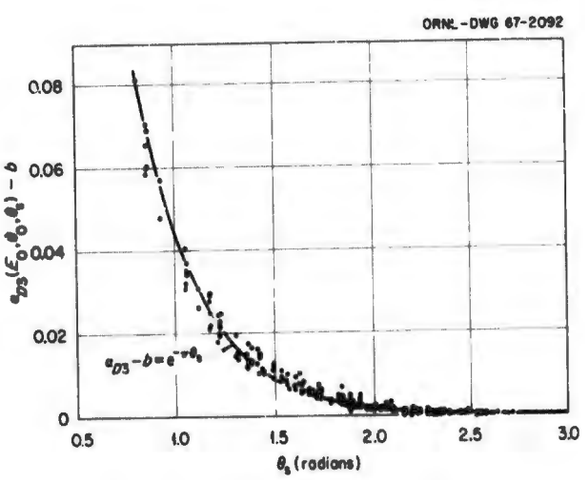

Fig. 4.40. Gamma-Ray Differential Dose Albedo for Aluminum, Iron, and Concrete as a Function of the Scattering Angle θ_s. (From Haggmark *et al.*, ref. 34.)

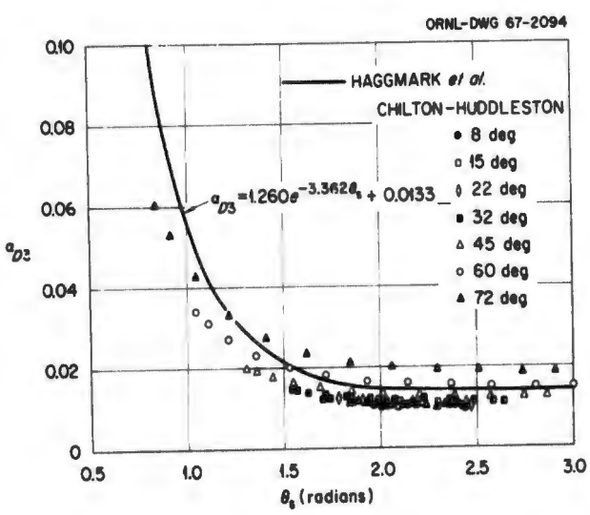

Fig. 4.42. Comparison of Gamma-Ray Differential Dose Albedos for Concrete Obtained with Equation 4.42 and with Chilton-Huddleston Formula. ^{137}Cs gamma rays (0.662 MeV) incident on concrete at cos θ_0 = 0.5. (From Haggmark *et al.*, ref. 34.)

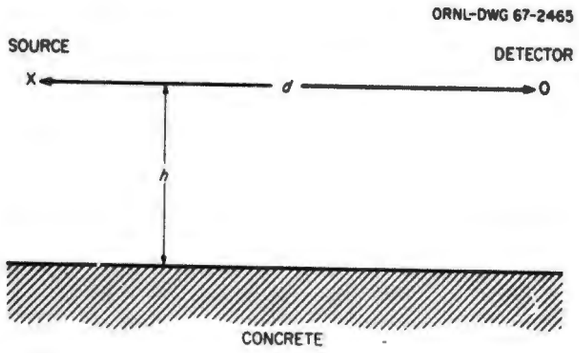

Fig. 4.43a. Geometry for Gamma-Ray Scattering Experiments Performed by Clarke and Batter.

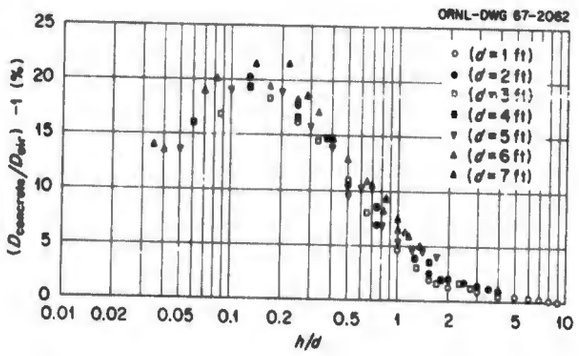

Fig. 4.43b. Increase in Gamma-Ray Dose Rate from a ^{192}Ir Source Due to Scattering from a Concrete Surface. Refer to Fig. 4.43a for experimental geometry. (From Clarke and Batter, ref. 36.)

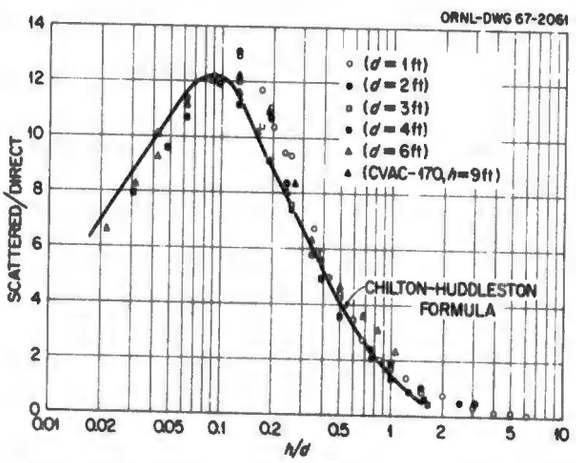

Fig. 4.43c. Ratio of Dose Rate from ^{60}Co Source Scattered from Concrete Surface to Direct Dose Rate. Refer to Fig. 4.43a for experimental geometry. (From Clarke and Batter, ref. 36.)

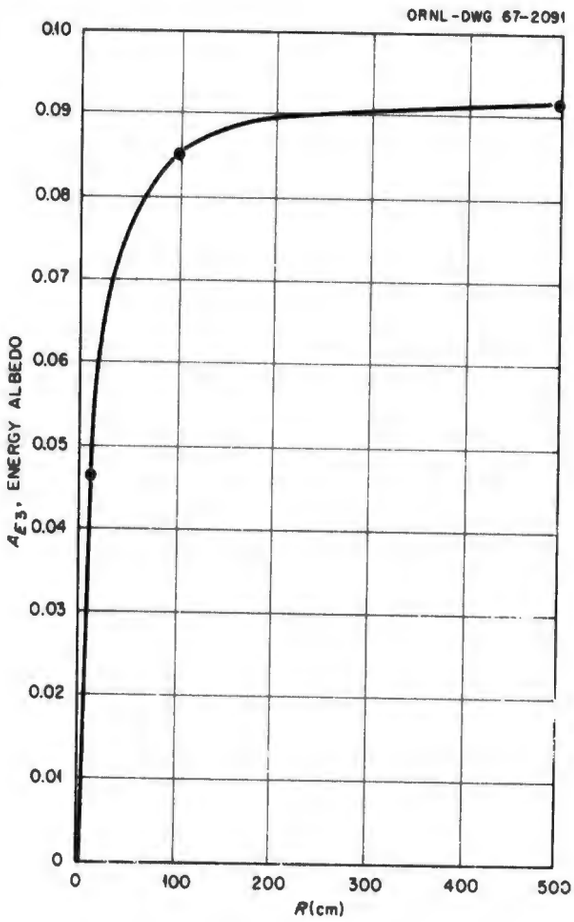

Fig. 4.44. Gamma-Ray Energy Flux Albedo as a Function of Radius of the Concrete Reflecting Wall (1-MeV Source). (From Leimdorfer, ref. 42.)

4.4 Secondary Gamma-Ray Albedos

Secondary gamma rays, that is, gamma rays produced by the interactions of neutrons with nuclei, can appreciably increase the number of gamma rays "reflected" from a material surface. The most important neutron interaction involved is absorption (radiative capture). In the absorption process the incident neutron combines with the target nucleus to form a compound nucleus which has an excitation energy equal to the binding energy of the neutron plus its kinetic energy. The compound nucleus is then usually de-excited by the prompt emission of gamma rays, commonly referred to as capture gamma rays. Of the various secondary gamma rays possible, capture gamma rays usually create the greatest problem for shielding designers, and therefore the few studies of secondary gamma-ray albedos that have been performed have largely been for capture gamma rays, as is evidenced by the discussion below.

Other secondary gamma rays which could be of concern in special situations are activation gamma rays and inelastic-scattering gamma rays. Activation gamma rays result when the absorption process leads to a radioactive residual nucleus which emits gamma rays at a later time. These gamma rays are of little consequence during a period of irradiation, but they can limit access to regions that have been close to a weapons burst. Inelastic-scattering gamma rays are produced when in a scattering process the incident neutron effectively transfers some of its energy to the target nucleus. This process is followed almost instantly by the release of gamma rays by the nucleus. Conceivably, inelastic-scattering gamma rays could be important contributors to secondary gamma-ray albedos, but generally this is not the case.

It is clear from the preceding discussion that the albedo definitions given in Section 4.1 do not apply precisely to the case of secondary gamma-ray albedos. To clarify the point that in this case the incident particles are neutrons and the emergent particles are gamma rays, the notation "(n,γ)" is included in the subscripts associated with the albedo symbols used below. In all cases the albedos are based on an incident particle current or flux and an emergent gamma-ray dose.

4.4.1. CAPTURE GAMMA-RAY ALBEDOS

In determining capture gamma-ray albedos, the capture gamma-ray source density within a medium must be known. The density at a point is given by

$$S_Y(E') = \sum_i \int \sigma_{ci}(E)\, Y_i(E')\, N_i\, \Phi(E)\, dE\,, \quad (4.43)$$

where

$\sigma_{ci}(E)$ = the capture cross section of element i for neutrons of energy E,
N_i = the atomic density of element i,
$\Phi(E)$ = the scalar neutron flux at energy E,
$Y_i(E')$ = the yield per capture in material i of gamma rays of energy E'.

Equation 4.43 enumerates the quantities which must be defined as a function of position within the absorbing material before gamma-ray leakage from the medium can be calculated. It also illustrates the number of parameters which must be duplicated in order for secondary gamma-ray data obtained for a particular situation to be applicable to another situation. In many cases sufficient accuracy will be obtained by considering only the total thermal-neutron flux profile and the capture cross sections averaged over the thermal group.

The data on capture gamma-ray albedos are quite limited. Wells[17] performed a series of Monte Carlo calculations from which he obtained capture gamma-ray albedos for the portland and TSF concrete compositions given in Table 4.9. Assuming that only thermal neutrons were incident, he arrived at the following expressions for the differential dose albedo, which is given in (rads hr^{-1} $steradian^{-1}$)/(unit thermal-neutron flux) incident at angle θ_0:

$$\alpha_{D1(n,\gamma)}(\theta_0,\theta) = 6.986 \times 10^{-8} \cos\theta_0 \cos\theta \quad (4.44)$$

for portland concrete and

$$\alpha_{D1(n,\gamma)}(\theta_0,\theta) = 1.046 \times 10^{-7} \cos^{5/4}\theta_0 \cos^{2/3}\theta \quad (4.45)$$

for TSF concrete. It is seen from these two expressions that for normal incidence and reflection

the capture gamma-ray albedo for the TSF concrete is greater than that for portland concrete by about 50%. In calculating the capture gamma-ray dose rate along the axis of a concrete-lined cylindrical hole, Wells found that the results obtained with the TSF albedo were higher by a factor of 1.4 to 1.5 than those obtained with the albedo for portland concrete. This demonstrates how variations in local aggregates used in site construction can cause variations in the capture gamma-ray albedo due to changes in both capture density and gamma-ray yield per capture.

Maerker and Muckenthaler[19] also obtained capture gamma-ray dose albedos from Monte Carlo calculations for thermal neutrons incident on concrete. In their case the concrete was assumed to be a five-region slab which contained steel in two regions (described in Section 4.2.2). The differential albedo data were fit to the expression

$$\alpha_{D2(n,\gamma)} = \mu^{2/3}(1.01 + 1.67\mu_0 - 0.56\mu_0^2) \times 10^{-7} , \quad (4.46)$$

where α_{D2} is given (rads hr^{-1} steradian^{-1})/(incident unit thermal-neutron current) and μ_0 and μ are the cosines of the incident and reflected polar angles respectively. The corresponding expression for the total albedo is

$$A_{D2(n,\gamma)} = 3.77 \times 10^{-7}(1.01 + 1.67\mu_0 - 0.56\mu_0^2) , \quad (4.47)$$

given in (rads/hr)/(incident unit thermal-neutron current). These equations fit the Monte Carlo data to within 15%.

Figure 4.45 compares the differential albedos obtained with the Maerker-Muckenthaler expression with those obtained with the Wells expression for TSF concrete, the latter being converted to type 2 albedos. The data differ by a factor of ~2, which may have resulted from several causes. In the Wells calculations neutron histories were terminated after 50 collisions, whereas 200 collisions were allowed in the Maerker and Muckenthaler calculations. According to additional studies performed by Maerker and Muckenthaler[19] and also by Coleman *et al.*,[8] however, this would account for no more than 20% of the difference. Other differences may appear in the gamma-ray yields, the minimum gamma-ray energy considered, and the concrete composition. In particular, the layered concrete slab used by Maerker and Muckenthaler had more iron nearer the surface than did the homogenized system used by Wells. The additional iron at this position probably resulted in more iron-capture gamma rays emerging from the surface.

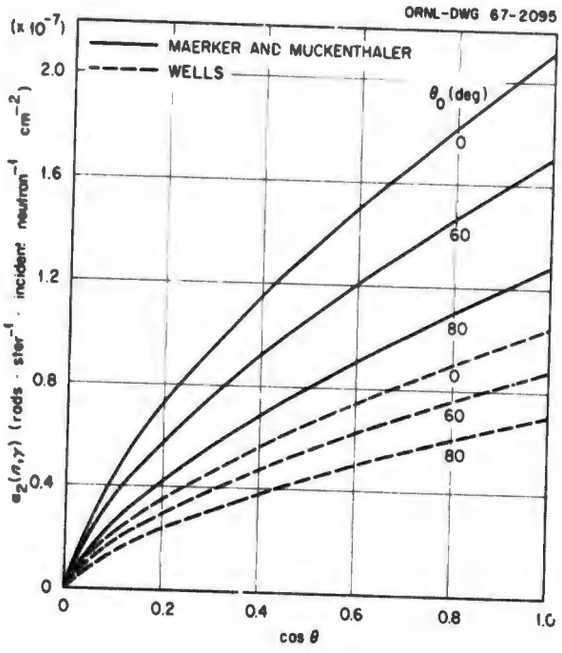

Fig. 4.45. Capture Gamma-Ray Differential Albedos for Thermal Neutrons Incident on Concrete. (From Wells, ref. 17, and Maerker and Muckenthaler, ref. 19.)

Coleman *et al.*[8] calculated, also by Monte Carlo methods, the capture gamma-ray albedos resulting from the slowing down and capture of neutrons incident on concrete at intermediate energies (0.5 eV to 200 keV). As was the case for the Maerker and Muckenthaler calculations, the concrete was assumed to be a five-region slab, with two of the regions containing steel; however, at most the iron contributed only 20% of the capture gamma-ray dose.

The empirical equations representing the results of Coleman *et al.* are shown in Table 4.17. The departure from unity of the last term in parentheses in the expressions for the differential albedos reflects the contributions from captures occurring at nonthermal energies. These expressions reproduce the Monte Carlo values to within 15% for the differential albedos and to within 10% for the total albedos.

Table 4.17. Curve-Fitted Expressions for Capture Gamma-Ray Differential and Total Albedos Arising from the Slowing Down and Capture of Incident Epicadmium Neutrons[a]

ΔE_0	$\alpha_{D2(n,\gamma)}(\Delta E_0, \mu_0, \mu)$[b] [(rads hr^{-1} steradian^{-1})/(incident unit neutron current)]	$A_{D2(n,\gamma)}(\Delta E_0; \mu_0)$ [(rads/hr)/(incident unit neutron current)]
55.1 – 200 keV	$10^{-7}\,\mu\,(0.43 + 2.17\mu - 1.67\mu^2)\,(0.39 + 0.51\mu_0)\,(1.10)$	$10^{-7}(1.40 + 1.83\mu_0)$
15.2 – 55.1 keV	$10^{-7}\,\mu\,(0.39 + 1.78\mu - 1.39\mu^2)\,(0.50 + 0.68\mu_0)\,(1.11)$	$10^{-7}(1.52 + 2.07\mu_0)$
4.2 – 15.2 keV	$10^{-7}\,\mu\,(0.70 + 2.53\mu - 2.07\mu^2)\,(0.37 + 0.46\mu_0)\,(1.12 - 0.01\mu_0)$	$10^{-7}(1.74 + 2.15\mu_0)$
1.15 – 4.2 keV	$10^{-7}\,\mu\,(0.68 + 2.59\mu - 2.08\mu^2)\,(0.40 + 0.54\mu_0)\,(1.12 - 0.01\mu_0)$	$10^{-7}(1.93 + 2.57\mu_0)$
0.32 – 1.15 keV	$10^{-7}\,\mu\,(0.66 + 3.18\mu - 2.60\mu^2)\,(0.46 + 0.54\mu_0)\,(1.14 - 0.02\mu_0)$	$10^{-7}(2.43 + 2.79\mu_0)$
87 – 320 keV	$10^{-7}\,\mu\,(0.89 + 3.52\mu - 3.09\mu^2)\,(0.41 + 0.59\mu_0)\,(1.18 - 0.06\mu_0)$	$10^{-7}(2.56 + 3.42\mu_0)$
24 – 87 eV	$10^{-7}\,\mu\,(1.14 + 3.98\mu - 3.77\mu^2)\,(0.38 + 0.62\mu_0)\,(1.30 - 0.15\mu_0)$	$10^{-7}(2.95 + 4.20\mu_0)$
6.6 – 24 eV	$10^{-7}\,\mu\,(1.40 + 2.73\mu - 2.50\mu^2)\,(0.45 + 0.65\mu_0)\,(1.11 - 0.04\mu_0)$	$10^{-7}(3.08 + 4.18\mu_0)$
1.8 – 6.6 eV	$10^{-7}\,\mu\,[1.34 + 0.78\mu_0 + \mu\,(0.15 + 2.30\mu_0) - \mu^2(0.60 + 2.11\mu_0)] \times (1.09 - 0.03\mu_0)$	$10^{-7}(3.89 + 4.14\mu_0)$
0.5 – 1.8 eV	$10^{-7}\,\mu\,[2.12 + 0.72\mu_0 + \mu\,(-1.46 + 2.92\mu_0) + \mu^2(0.40 - 2.68\mu_0)] \times (1.07 - 0.02\mu_0)$	$10^{-7}(4.52 + 4.33\mu_0)$

[a]Table taken from: W. A. Coleman, R. E. Maerker, F. J. Muckenthaler, and P. N. Stevens, *Nucl. Sci. Eng.* 27, 411–422 (1967).

[b]$\mu_0 = \cos\,\theta_0$; $\mu = \cos\,\theta$.

Wells and Tompkins[43] calculated the capture gamma-ray dose rate at a point 3 ft above the surface of several materials that was due to an incident spectrum of neutrons, including fast neutrons, from reactor and weapon sources. The materials considered were Nevada Test Site (NTS) soil, TSF concrete, TSF sandy soil, and sea water. Calculations of the production of capture gamma rays within the materials were based on experimentally determined thermal-neutron fluxes as a function of depth in the material.

The calculational geometry used by Wells and Tompkins is shown in Fig. 4.46*a*. The detector was assumed to be located at *P*, and a point kernel program[44] was used to calculate the angular dose distribution arriving at *P*. After normalization to a unit thermal-neutron flux uniformly incident over the surface of the absorbing plane, the results were found to fit a function of the form

$$D(\theta) = C \cos^n \theta\,. \qquad (4.48)$$

Values of *C* and *n* are shown in Table 4.18 for the materials used in the analysis. Figure 4.46*b* is a cumulative plot of the capture gamma-ray dose rate as a function of θ for the TSF concrete, and Fig. 4.46*c* is a similar plot for the NTS soil.

A more precise calculation was carried out by French, Wells, and Schaeffer[45] for the case of the TSF concrete. The capture gamma-ray source strength as a function of depth was determined in the same manner as described for the Wells and Tompkins calculations, but the gamma-ray leakage

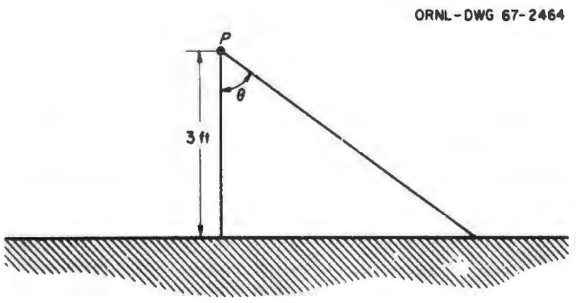

Fig. 4.46*a*. Geometry for Calculating Capture Gamma-Ray Dose at a Point 3 ft Above Material Surface.

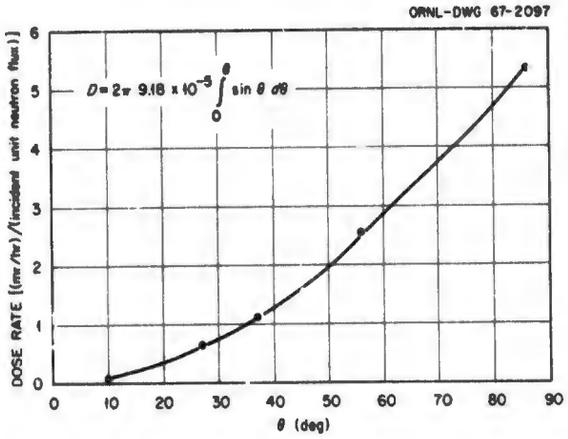

Fig. 4.46b. Cumulative Capture Gamma-Ray Dose Rate 3 ft Above TSF Concrete Due to Unit Thermal-Neutron Flux Incident on Concrete Surface. (From Wells and Tompkins, ref. 43.)

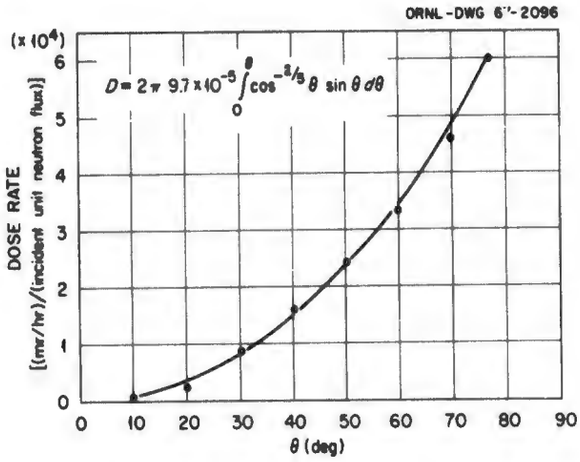

Fig. 4.46c. Cumulative Capture Gamma-Ray Dose Rate 3 ft Above Nevada Test Site Soil Due to Unit Thermal-Neutron Flux Incident on Soil Surface. (From Wells and Tompkins, ref. 43.)

Table 4.18. Values of Constants Required for Calculating Capture Gamma-Ray Dose Rates by Eq. 4.48

Material	Density (g/cm^3)	C	n	Reference
TSF sandy soil	1.469	8.9×10^{-5}	$-\frac{2}{3}$	*a*
TSF concrete	2.41	9.18×10^{-5}	0	*b*
Nevada test site soil	1.18	9.7×10^{-5}	$-\frac{2}{5}$	*c*
Sea water	1.025	1.37×10^{-4}	$-\frac{1}{4}$	*d*

[a]W. C. Farries and J. R. Stokes, *Postanalysis of Ordnance Corps Radiologically Protected Pod Tests at ORNL-TSF*, General Dynamics/Fort Worth Report FZK-145 (1962) (Secret).

[b]V. R. Cain, *A Study of the Radiation Shielding Characteristics of Basic Concrete Structures at the Tower Shielding Facility*, Oak Ridge National Laboratory Report ORNL-3464 (1964).

[c]C. S. Cook, W. E. Thompson, F. M. Tomnovic, R. L. Mather, J. M. Ferguson, and P. R. Howland, *Operation Plumbob, Project 2.2, Neutron-Induced Activities in Soil Elements*, Defense Atomic Support Agency Report WT-1411 (1959) (Secret).

[d]W. A. Biggers and F. Waddell, *General Report on Weapons Tests, External Neutron Measurements, 1946–1956*, Los Alamos Scientific Laboratory Report WT-9004, p. 167 (1957) (Secret).

from the concrete was calculated by using the C-18 Monte Carlo code.[46] The resulting angular dose rates, in rads hr^{-1} $steradian^{-1}$, were found to fit an equation of the form

$$D(\theta) = 6.14 \times 10^{-8} \cos\theta\ . \qquad (4.49)$$

This equation gives dose rates that are approximately 24% lower than those obtained with Eq. 4.48.

Capture gamma-ray dose rates for materials similar to those studied by Tompkins and Wells and by French *et al.* may be approximated from the equation

$$D = \int D(\theta)\ \Phi\ d\Omega\ , \qquad (4.50)$$

where $\Phi\ D(\theta)$ is obtained by either Eq. 4.48 or 4.49.

A somewhat different approach was used by Budka *et al.*[47–49] for calculating the reflection of capture gamma rays from slabs of concrete and NTS soil. In their calculations, which were performed with the GRATIS Monte Carlo program[47] and included transmission through the slab as well as reflection from it, the independent variables were the energy and distribution of the secondary gamma-ray sources rather than the energy of the

incident neutron. Leakage from both slab faces was calculated for gamma-ray source distributions represented by the function

$$N_j(x) = \bar{x}^k , \qquad (4.51)$$

where $\bar{x}$ refers to the depth within a slab expressed as the fraction of the total slab thickness T (i.e., $\bar{x} = x/T$), and $N_j(\bar{x})\, d\bar{x}$ represents the estimated number of gamma rays of energy E_j originating at depth x to $x + dx$ centimeters from the reflecting surface. The fractional dose leaking from the slab per source photon was calculated for $k = 0, 1, 2, 3,$ and 4 for slab thicknesses of 1, 2, 4, 8, 12, 16, and 20 in. for monoenergetic photon energies between 1.0 and 11.0 MeV.

While the results obtained from this type of calculation are not n,γ albedo data *per se*, they may be used to obtain effective albedo data for an incident neutron current or flux provided that the distribution of gamma-ray sources within the slab is known and that this distribution can be reasonably approximated by the polynomial expression

$$N_j(\bar{x}) = A_{0j} + a_{1j}\bar{x} \ldots + a_{4j}\bar{x}^4 . \qquad (4.52)$$

The coefficients a_{kj} related to the weighting functions for the individual results for the $\bar{x}^k$ distributions and must be determined such that the total number (or dose) leaving the reflecting surface will be given by

$$t_R = \frac{\sum_{j=1}^{M} \sum_{k=0}^{K} r_{jk}\, a^*_{kj}}{\sum_{j=1}^{M} \sum_{k=0}^{K} a^*_{kj}} . \qquad (4.53)$$

Here a^*_{kj} represents a correction due to the error introduced by using a polynomial fit of the form of Eq. 4.52 and is given by

$$a^*_{kj} = \frac{N_j}{\bar{N}_j} \frac{a_{kj}}{k+1} , \qquad (4.54)$$

where $\bar{N}_j$ is the estimated number of photons originating in the slab, as opposed to N_j, which is the actual number. The term r_{jk} in Eq. 4.53 is the data calculated by Budka *et al.*: the reflected current of capture gamma rays of initial energy E_j having a source depth distribution $\bar{x}^k$. The weighting functions are the polynomial coefficients which give an equation approximating the capture depth distribution and which have been normalized such that the integral of the polynomial over the slab depth yields the total number of captures. Similar weighting functions may be developed for the dose transmission data. Small changes in material composition may be accounted for in terms of their influence on the thermal-neutron flux profile and capture spectrum if they do not greatly influence the gamma-ray attenuation properties.

Some of the data on reflected dose for the case of concrete of the composition shown in Table 4.19 are presented in Figs. 4.47 through 4.51. The "fraction reflected" in these curves refers to the ratio of reflected dose near the slab face to the dose which would be found at the same point in the absence of the gamma-ray attenuating material (that is, the source dose). For the assumed infinite-slab condition, values of the source dose are independent of the source depth distribution. Figure 4.52 gives the source dose as a function of source energy.

It is emphasized that the data calculated by Budka *et al.* will not be appreciably influenced by expected variations in concrete composition if thicknesses are scaled in accordance with the density. The weighting constants used in application of the data will, however, be very sensitive to composition.

A complete listing of the energy and angular distribution of the transmitted and reflected gamma rays may be obtained from ref. 48 for concrete and from ref. 49 for the NTS soil.

Table 4.19. Composition of Concrete ($\rho = 2.3$ g/cm^3) Used in Calculations by Budka *et al.*

Compound	Composition (wt %)
SiO_2	64
Al_2O_3	10
Fe_2O_3	2
$CaCO_3$	1
Na_2O	3
K_2O	3
H_2O	9
MgO	1
CaO	7

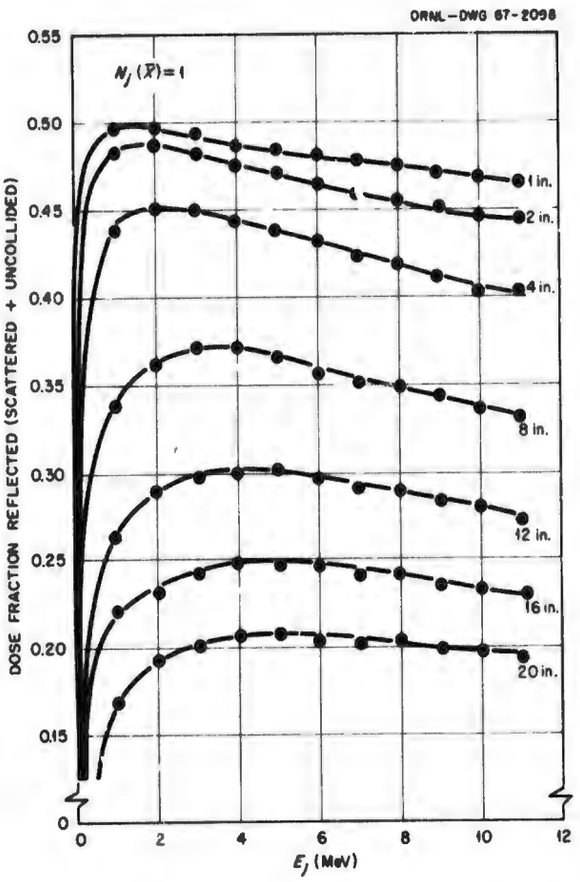

Fig. 4.47. Fraction of Capture Gamma-Ray Dose Reflected from Concrete Slab as a Function of the Source Energy $[N_j(\bar{x}) = 1]$. (From Budka and Dolce, ref. 49.)

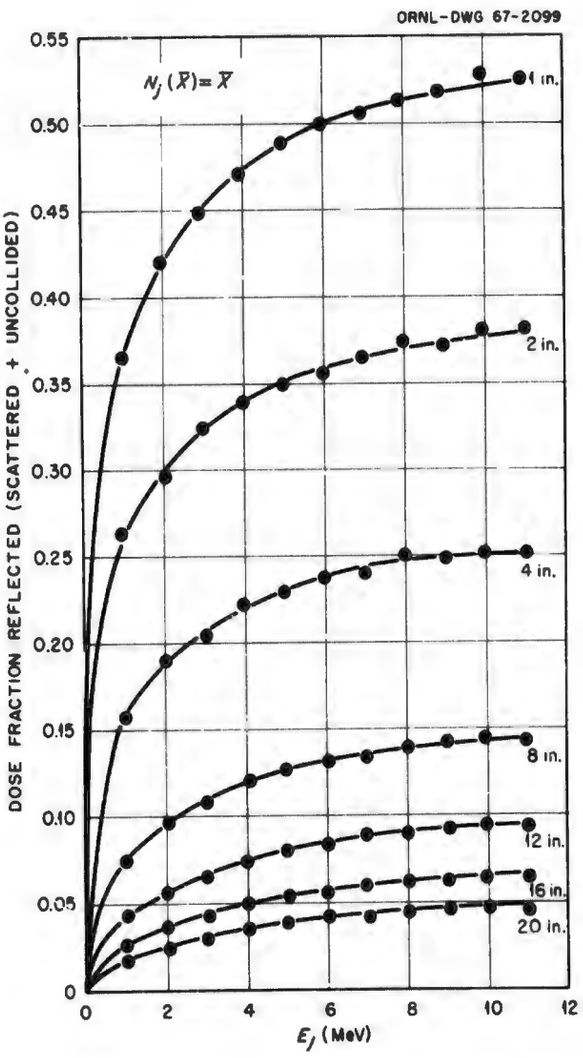

Fig. 4.48. Fraction of Capture Gamma-Ray Dose Reflected from Concrete Slab as a Function of the Source Energy $[N_j(\bar{x}) = \bar{x}]$. (From Budka and Dolce, ref. 49.)

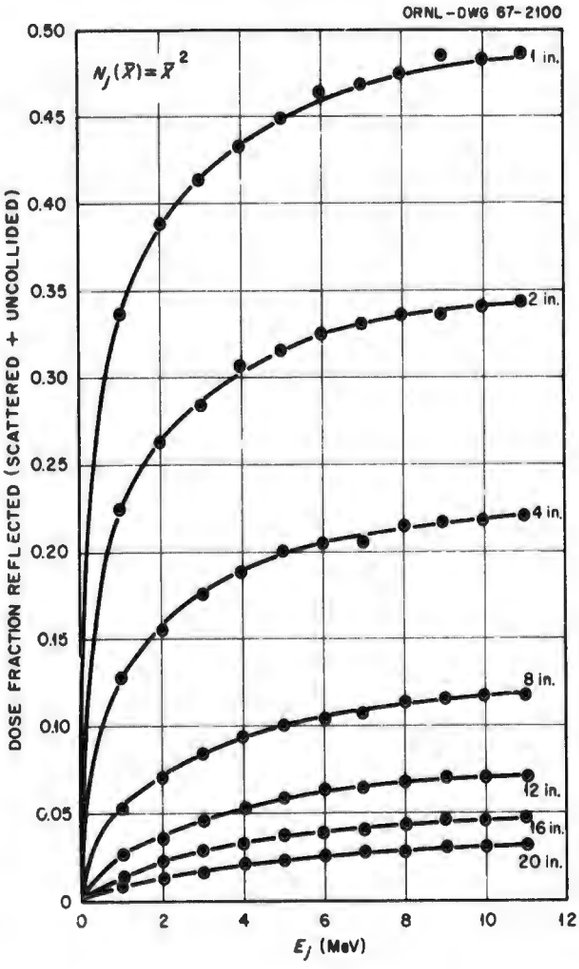

Fig. 4.49. Fraction of Capture Gamma-Ray Dose Reflected from Concrete Slab as a Function of the Source Energy $[N_j(\bar{x}) = \bar{x}^2]$. (From Budka and Dolce, ref. 49.)

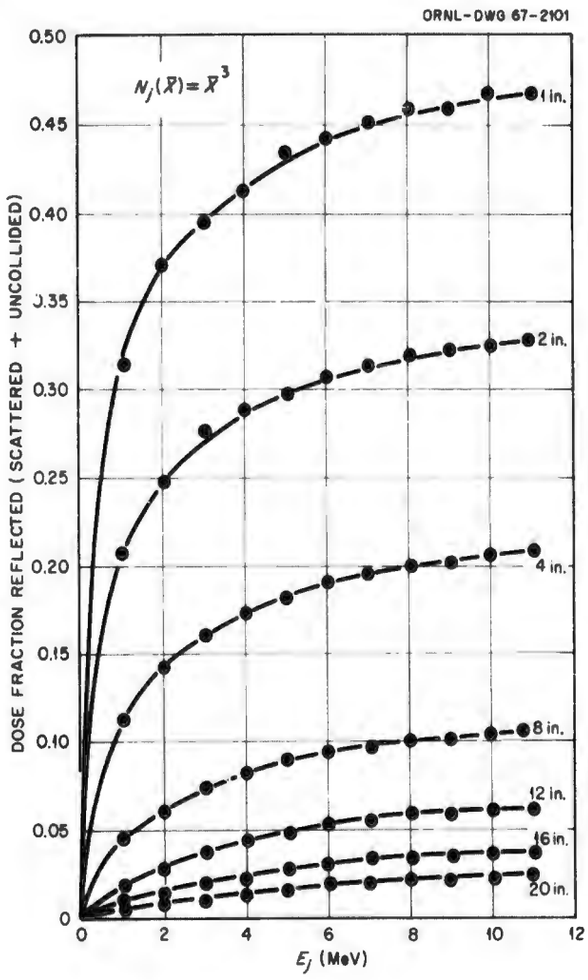

Fig. 4.50. Fraction of Capture Gamma-Ray Dose Reflected from Concrete Slab as a Function of the Source Energy $[N_j(\bar{x}) = \bar{x}^2]$. (From Budka and Dolce, ref. 49.)

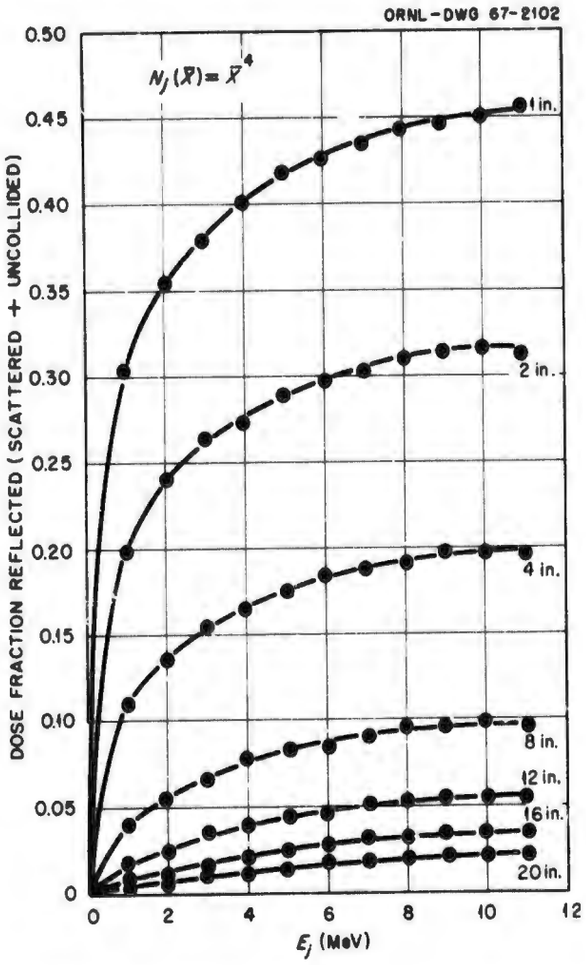

Fig. 4.51. Fraction of Capture Gamma-Ray Dose Reflected from Concrete Slab as a Function of the Source Energy $[N_j(\bar{x}) = \bar{x}^4]$. (From Budka and Dolce, ref. 49.)

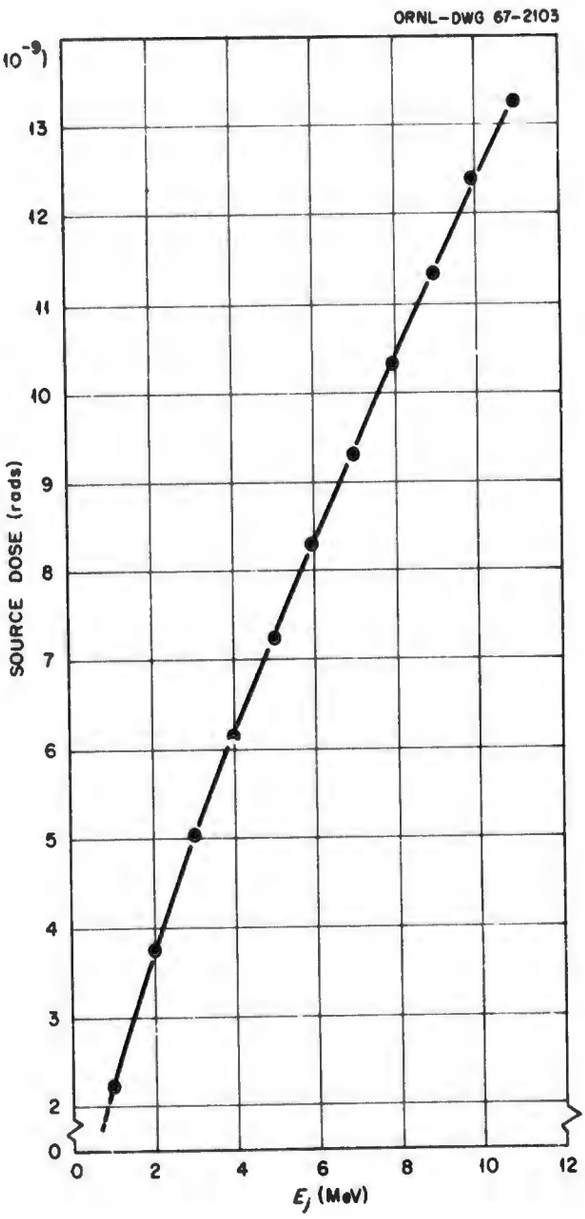

Fig. 4.52. Capture Gamma-Ray Source Dose vs Source Energy. (From Budka and Dolce, ref. 49.)

4.4.2. ACTIVATION GAMMA-RAY ALBEDOS

The subject of neutron activation of a material is treated in Chapter 2 in the section on residual radiation. It is mentioned here only to call attention to the fact that activation results in the emission of decay gamma rays, which may be described in terms of an n,γ albedo. An important difference between this type of albedo and a neutron-capture albedo is the time delay between the incident neutrons and emergent gamma rays.

As in the case of capture gamma rays, activation gamma rays are primarily a product of thermal-neutron absorption and thus will be determined by the thermal-neutron flux intensity. Activation gamma rays will not add appreciably to the total dose measured by a detector that remains stationary throughout the evolution of a weapon detonation; however, it will be the most intense component to be considered in occupying terrain near the location where the detonation occurred.

4.4.3. INELASTIC-SCATTERING GAMMA-RAY ALBEDOS

As was mentioned earlier, when a neutron scatters inelastically, part of its energy is absorbed by the target nucleus, raising the nucleus to an excited state. An intermediate step may be the formation of a short-lived compound nucleus by union of the target nucleus and incident neutron. In any case the extra neutron is either scattered or ejected from the nucleus, which then decays back to its ground state by the emission of gamma rays. The time between the neutron interaction and the gamma-ray emission is negligible (10^{-14} sec). If the energy of the incident neutron is insufficient to raise the target nucleus to its first excited state, inelastic scattering cannot occur.

Cross sections for inelastic scattering are not well known. They are complicated by the multiplicity of levels to which the target nucleus may be excited and the multiplicity of gamma-ray energies which may be emitted in the process of decay from a given energy level. As the neutron energy increases, so does the number of nuclear levels. When the energy of the incident neutron exceeds about 4 MeV, the gamma-ray emission spectrum becomes essentially continuous for most scattering species.

The emission of inelastic scattering gamma rays from a surface on which weapons neutrons are incident will not add significantly to the reflected dose rate; however, the gamma rays produced by inelastic scattering may constitute the most penetrating component of the reflected dose (that is, they may have the highest energies). Thus if it is planned to shield against the gamma rays reflected from a material, the inelastic-scattering component should be considered.

No albedo data are available either from experiments or from analyses for use in estimating inelastic gamma-ray return from various materials. Preliminary estimates may be made by using a single-scattering approximation, and more sophisticated calculations may be made by a Monte Carlo approach. In either case the outcome would depend on the availability of appropriate cross-section data, and at this time there are many gaps in such data. The data that are available are maintained in a central file by the Sigma Center at Brookhaven National Laboratory. Compilations have also been published for some elements by United Nuclear Corporation.[50] In addition, a summary of neutron energy thresholds and possible gamma-ray energies has been given by Goldstein.[51]

References

[1]R. E. Maerker and F. J. Muckenthaler, "Calculation and Measurement of the Fast-Neutron Differential Dose Albedo for Concrete," *Nucl. Sci. Eng.* **22**, 455 (1965).

[2]F. J. Allen, A. Futterer, and W. Wright, *Neutron Reflection and Flux Versus Depth for Nevada Test Site Soil*, Ballistic Research Laboratories Report BRL-1190 (January 1963); ... *for Concrete*, Ballistic Research Laboratories Report BRL-1189 (January 1963); ... *for Iron*, Ballistic Research Laboratories Report BRL-1199 (March 1963); *Neutron Reflection and Flux Versus Depth for Water, with an Appendix, Comparison of Results of National Bureau of Standards*, Ballistic Research Laboratories Report BRL-1204 (June 1963); *Neutron Reflection and Flux Versus Depth for Aluminum with an Appendix: Neutron Dose Transmission Versus Thickness*, Ballistic Research Laboratories Report BRL-1238 (February 1964); and *Angular Distributions and Energy Spectra of Neutrons Transmitted Through Polyethylene*, Ballistic Research Laboratories Report BRL-1148 (classified) (September 1961).

[3]F. J. Allen, A. Futterer, and W. Wright, *Dependence of Neutron Albedos upon Hydrogen Content of a Shield*, Ballistic Research Laboratories Report BRL-1224 (October 1963).

[4]R. L. French and M. B. Wells, *An Angular Dependent Albedo for Fast-Neutron Reflection Calculations*, Radiation Research Associates Report RRA-M31 (November 1963).

[5]Y. T. Song, *Fast Neutron Streaming Through Two-Legged Concrete Ducts*, U.S. Naval Civil Engineering Laboratory Report NCEL-TR-354 (Feb. 2, 1965).

[6]A. B. Chilton and C. M. Huddleston, *A Semiempirical Formula for Differential Dose Albedo for Gamma Rays on Concrete*, U.S. Naval Civil Engineering Laboratory Report, NCEL-TR-228 (Nov. 16, 1962); also, *Nucl. Sci. Eng.* **17**, 419 (1963).

[7]R. L. Henry, L. G. Mooney, and R. J. Provost, *Study of Radiation Penetration and Reflection from Shield Materials*, General Dynamics/Fort Worth Report FZK-183 (August 1964).

[8]W. A. Coleman, R. E. Maerker, F. J. Muckenthaler, and P. N. Stevens, "Calculation of Doubly Differential Current Albedos for Epicadmium Neutrons Incident on Concrete and Comparison of the Reflected Subcadmium Component with Experiment," *Nucl. Sci. Eng.* **27**, 411 (1967).

[9]E. Fermi, *On the Motion of Neutrons in Hydrogenous Substances*, NP-2385 [translated from *Ric. Sci.* VII(2), 13 (1936)].

[10]O. Halpern, R. Lueneburg, and O. Clark, "On Multiple Scattering of Neutrons. I. Theory of the Albedo of a Plane Boundary," *Phys. Rev.* **53**, 173 (1938).

[11]S. Glasstone and M. C. Edlund, *The Elements of Nuclear Reactor Theory*, Van Nostrand, New York, 1952.

[12]S. Chandrasekhar, *Radiative Transfer*, Clarendon Press, Oxford, 1950.

[13]L. V. Spencer, J. A. Diaz, and E. Moses, *Neutron Penetration in Cylindrical Ducts*, National Bureau of Standards Report NBS-8542 (Sept. 1, 1964).

[14]A. Mockel, "Reflection and Transmission by a Strongly Absorbing Slab," *Nucl. Sci. Eng.* **22**, 339 (1965).

[15]R. Bellman, R. Kalaba, and M. Prestrud, *Invariant Imbedding and Radiative Transfer in Slabs of Definite Thickness*, American Elsevier Publishing Co., New York, 1963.

[16]G. C. Pomraning, "The Albedo Problem," *Nucl. Sci. Eng.* **21**, 265 (1965).

[17]M. B. Wells, *Reflection of Thermal Neutrons and Neutron-Capture Gamma Rays from Concrete*, Radiation Research Associates Report RRA-M44 (June 1954).

[18]M. B. Wells, *Gamma Dose Rates Resulting from Neutron Capture in Air and Concrete*, Convair/Fort Worth Report, NARF-59-31T (September 1959).

[19]R. E. Maerker and F. J. Muckenthaler, "Measurements and Single-Velocity Calculations of Differential Angular Thermal-Neutron Albedos for Concrete," *Nucl. Sci. Eng.* **26**, 339 (1966).

[20]H. Greenspan and I. G. Baksys, *Addenda to Newsletters No. 3 and 4*, Argonne National Laboratory Newsletter No. 9 (TID-18481) (March 1963).

[21]C. M. Davisson and R. D. Evans, "Gamma-Ray Absorption Coefficients," *Revs. Mod. Phys.* **24**, 79 (1952).

[22]M. Leimdorfer, *The Backscattering of Gamma Radiation from Plane Concrete Walls*, Aktiebolaget Atomenergi Report AE-92 (December 1962).

[23]M. B. Wells, *Differential Dose Albedos for Calculation of Gamma-Ray Reflection from Concrete*, Radiation Research Associates Report RRA-T46 (December 1964).

[24]J. M. Berger and J. Doggett, "Reflection and Transmission of Gamma Radiation by Barriers: Semianalytic Monte Carlo Calculations," *J. Res. Natl. Bur. Std.* **56**, 89 (1956).

[25]M. J. Berger and D. J. Raso, "Monte Carlo Calculations of Gamma-Ray Backscattering," *Radiation Res.* **12**, 20 (1960).

[26]M. J. Berger and D. J. Raso, *Backscattering of Gamma Rays*, National Bureau of Standards Report NBS-5982 (July 25, 1958).

[27]D. J. Raso, "Monte Carlo Calculations on the Reflection and Transmission of Scattered Gamma Rays," *Nucl. Sci. Eng.* **17**, 411 (1963).

[28]M. B. Wells, *Air and Concrete Scattering of Gamma Rays*, Convair/Fort Worth Report MR-N-229 (NARF-59-11T) (March 1959).

[29]A. B. Chilton, C. M. Davisson, and L. A. Beach, "Parameters for C-H Albedo Formula for Gamma Rays Reflected from Water, Concrete, Iron, and Lead," *Trans. Am. Nucl. Soc.* **8**, 656 (1965).

[30]C. M. Davisson and L. A. Beach, "A Monte Carlo Study of Back-Scattered Gamma Radiation," *Trans. Am. Nucl. Soc.* **5**, 391 (1962).

[31]A. B. Chilton, "A Modified Exposure Albedo Formula for Gamma Rays Reflected from Concrete," *Trans. Am. Nucl. Soc.* **9**, 369 (1966).

[32]M. J. Berger and E. E. Morris, *Dose Albedo and Transmission Coefficients for Cobalt-60 and Cesium-137 Gamma Rays Incident on Concrete Slabs*, National Bureau of Standards Report NBS-9071 (July 5, 1966).

[33]C. E. Clifford, *Differential Dose Albedo Measurements for 0.66 MeV γ's Incident on Concrete, Iron and Lead*, Defense Research Chemical Laboratories, Ottawa, Report DRCL-412 (August 1963).

[34]L. G. Haggmark *et al.*, "Differential Dose-Rate Measurements of Backscattered Gamma Rays from Concrete, Aluminum and Steel," *Nucl. Sci. Eng.* **23**, 138 (1965).

[35]M. J. Barrett and J. Waldman, *Experimental Gamma-Ray Backscattering by Various Materials*, Technical Operations Research Report TO-B 64–68 (July 1964).

[36]E. T. Clarke and J. F. Batter, "Gamma-Ray Scattering by Concrete Surfaces," *Nucl. Sci. Eng.* **17**, 125 (1963).

[37]B. L. Jones *et al.*, *Air and Ground Scattering of Cobalt-60 Gamma Radiation*, Consolidated Vultee Aircraft Corporation Report CVAC-170 (Mar. 30, 1955).

[38]A. B. Chilton, *Backscattering of Gamma Rays from a Point Source Near a Concrete Plane Surface*, University of Illinois Engineering Experimental Station Bulletin 471 (1964).

[39]W. R. Hendee and J. L. Ellis, "Scattering of Gamma Radiation from Semi-Infinite Slabs," *Health Phys.* **12**, 673 (1966).

[40]D. G. Andrews and J. J. Steyn, "Experimental Differential Number, Energy and Dose Albedos for Semi-Infinite Media, for Normally-Incident Gamma Radiation," *Trans. Am. Nucl. Soc.* **8**, 655 (1965).

[41]C. Eisenhauer, "An Image Source Technique for Calculating Reflection of Gamma Rays or Neutrons," *Health Phys.* **11**, 1145 (1965).

[42]M. Leimdorfer, *Backscattering of Gamma Radiation from Spherical Concrete Walls*, Aktiebolaget Atomenergi Report AE-93 (January 1963).

[43]M. B. Wells and K. W. Tompkins, unpublished data.

[44]D. M. Peterson, *Shield Penetration Programs C-17 and L-63*, General Dynamics/Fort Worth Report NARF-61-39T (Dec. 29, 1961).

[45]R. L. French, M. B. Wells, and N. M. Schaeffer, *Penetration of Neutron and Gamma Radiation Through the Openings of Underground Structures*, Radiation Research Associates Report RRA-T41 (Nov. 30, 1964).

[46]M. B. Wells, *Radiation Resistant Combat Vehicle Investigation – Final Report, Volume III: Monte Carlo Multilayer Slab Geometry Shielding Code C-18*, General Dynamics/Fort Worth Report FZK-134-3 (Secret).

[47]A. J. Budka, *Gratis – A Monte Carlo Computer Program for Calculating Transmission Information for Secondary Gamma Radiation*, Ballistics Research Laboratories Report BRL-1223 (October 1963).

[48]A. J. Budka and T. Dolce, *Secondary Gamma Ray Transmission Through Plane Slabs of Concrete*, Ballistic Research Laboratories Report BRL-1307 (September 1965).

[49]A. J. Budka, W. Brand, and T. Dolce, *Secondary Gamma Ray Transmission Through Nevada Test Site Soil*, Ballistic Research Laboratories Report BRL-1329 (July 1966).

[50]N. Tralli *et al.*, *Fast Neutron Cross Sections for Titanium, Potassium, Magnesium, Nitrogen,*

Aluminum, Silicon, Sodium, Oxygen, and Manganese – Final Report, United Nuclear Corporation Report UNC-5002 (NDL-TR-30) (January 1962); A. D. Krumbein, *Neutron Cross Sections for Beryllium*, United Nuclear Corporation Report UNC-5014, Vol. B (NDL-TR-36, Vol. B) (May 1962); and M. H. Kalos, H. Goldstein, and J. Ray, *Revised Cross Sections for Neutron Interactions with Oxygen and Deuterium – Final Report*, United Nuclear Corporation Report UNC-5038 (NDL-TR-40) (Aug. 31, 1962).

[51]H. Goldstein, "Sources of Neutrons and Gamma Rays," Chapter 8 in *Shielding*, Part B, Vol. III of *Reactor Handbook*, edited by E. P. Blizard and L. S. Abbott, Interscience, New York, 1962.

Unclassified

Security Classification

DOCUMENT CONTROL DATA - R & D

(Security classification of title, body of abstract and indexing annotation must be entered when the overall report is classified)

1. ORIGINATING ACTIVITY *(Corporate author)*
Oak Ridge National Laboratory
Oak Ridge, Tennessee

2a. REPORT SECURITY CLASSIFICATION
Unclassified

2b. GROUP

3. REPORT TITLE
"Neutron and Gamma-Ray Albedos," Chapter 4 of Weapons Radiation Shielding Handbook

4. DESCRIPTIVE NOTES *(Type of report and inclusive dates)*
Handbook

5. AUTHOR(S) *(First name, middle initial, last name)*
Author: Wade E. Selph
Editors: Lorraine S. Abbott, H. Clyde Claiborne, and Charles E. Clifford

6. REPORT DATE	7a. TOTAL NO. OF PAGES	7b. NO. OF REFS
May 1967	48	51

8a. CONTRACT OR GRANT NO.	9a. ORIGINATOR'S REPORT NUMBER(S)
Interagency Agreement: 40-36-64	DASA-1892-2
b. PROJECT NO. DASA Task: A2-11.033	
c. IACRO EO 804-64	9b. OTHER REPORT NO(S) *(Any other numbers that may be assigned this report)*
d.	

10. DISTRIBUTION STATEMENT
Each transmittal of this document outside the agencies of the U.S. Government must have prior approval of Headquarters, Defense Atomic Support Agency.

11. SUPPLEMENTARY NOTES	12. SPONSORING MILITARY ACTIVITY
	Defense Atomic Support Agency Washington, D.C. 20301

13. ABSTRACT

Air-filled openings through weapons radiation shields (for example, ducts, passageways, etc.) can increase the total amount of radiation penetrating the shield, primarily as a result of radiation successively scattering from the walls of the openings. Most techniques that have been developed for estimating the transmission of radiation through such openings depend on the use of albedos, an albedo being the fraction of radiation incident on a surface that is reflected back out of the material, assuming that the radiation enters and emerges at the same point. This chapter of the Handbook surveys the work performed to date on the various types of nuclear radiation albedos and uses a consistent nomenclature which shows the relationship of the results obtained in the different studies. Since the material considered most often for weapons radiation shields is concrete, most of the albedo data are for this material, although some data have been obtained for other materials, particularly for soils. (U)

The data are reported as singly differential albedos (differential with respect to the emergent angle), doubly differential albedos (differential with respect to both the emergent energy and the emergent angle), and total albedos (albedos for which the data have been integrated over both the emergent energy and emergent angle). (U)

Three fundamental types of differential and total albedos are used: an albedo which represents an incident flux of particles and an emergent current of particles, an albedo which represents an incident current and an emergent current, and an albedo which represents an incident flux and an emergent flux. These fundamental albedos may be weighted by dose response functions or by energy. (U)

The albedo investigations have largely consisted of calculations, primarily Monte Carlo machine calculations; however, in many cases there has been sufficient experimental confirmation to establish the validity of the calculated data. In nearly all cases the calculated data have been fitted to empirical expressions. (U)

DD FORM 1 NOV 65 1473

Unclassified

Security Classification

Unclassified
Security Classification

In this chapter separate sections are devoted to neutron albedos, gamma-ray albedos, and secondary gamma-ray albedos. The neutron albedos are classified according to their emergent energies as fast-neutron albedos, intermediate-energy neutron albedos, and thermal-energy neutron albedos. The thermal albedos are further divided into thermal albedos for neutrons incident at thermal energies and thermal albedos for neutrons incident at higher energies. The section on secondary gamma-ray albedos discusses albedos for emergent gamma rays that result from incident neutrons. They are classified as capture gamma-ray albedos, activation gamma-ray albedos, and inelastic-scattering gamma-ray albedos. (U)

14. KEY WORDS	LINK A		LINK B		LINK C	
	ROLE	WT	ROLE	WT	ROLE	WT
Neutron Albedos						
Gamma-Ray Albedos						
Secondary Gamma-Ray Albedos						
Concrete Albedos						

Unclassified
Security Classification